[Short title + Author Name - P&H title] 17 (2024) 105707

Contents lists available at ScienceDirect

Arabian Journal of Chemistry

journal homepage: www.ksu.edu.sa

Original article

Binary and ternary approach of solubility of Rivaroxaban for preparation of developed nano drug using supercritical fluid

Mahshid Askarizadeh [a], Nadia Esfandiari [a,*], Bizhan Honarvar [a], Seyed Ali Sajadian [b,c], Amin Azdarpour [d]

[a] Department of Chemical Engineering, Marvdasht Branch, Islamic Azad University, Marvdasht, Iran
[b] Department of Chemical Engineering, Faculty of Engineering, University of Kashan, Postal Code, 87317-53153, Kashan, Iran
[c] South Zagros Oil and Gas Production, National Iranian Oil Company, Postal Code, 7135717991, Shiraz, Iran
[d] Department of Petroleum Engineering, Marvdasht Branch, Islamic Azad University, Marvdasht, Iran

ARTICLE INFO

Keywords:
Rivaroxaban
Solubility
Supercritical carbon dioxide
Semi-empirical modeling
Co-solvent

ABSTRACT

This study addressed the solubility of Rivaroxaban in supercritical carbon dioxide at a temperature range of 308–338 K and a pressure range of 12–30 MPa with and without a Co-solvent in binary and ternary systems. The impact of ethanol Co-solvent was also examined. Furthermore, the examined systems were modeled using semi-empirical approaches once the tentative solubility data were determined. Rivaroxaban solubility in the binary and ternary systems ranged based on mole fraction from 1.0×10^{-6} to 2.57×10^{-5} and 1.9×10^{-5} to 2.02×10^{-4}, respectively. Based on the results, the use of a Co-solvent can greatly boost the solubility of Rivaroxaban. The highest Co-solvent effect on the Rivaroxaban-Ethanol-CO_2 mixture was observed at 18.73 (338 K and 12 MPa). Furthermore, empirical and semi-empirical models can effectively fit the solubility values of the analyzed materials by AARD% and R_{adj} for binary and ternary approaches. The Jouyban *et al.* (AARD%=7.40 and R_{adj} = 0.993) model for the binary system and the Garlapati-Madras (AARD%=6.16 and R_{adj} = 0.991) and Sodeifian-Sajadian (AARD%=6.13 and R_{adj} = 0.979) and Soltani-Mazloumi (AARD%=6.89 and R_{adj} = 0.987) models for the ternary system are the most accurate models.

1. Introduction

Rivaroxaban (RXN) is the first authorized oral direct factor Xa inhibitor (xabans) and a direct oral anticoagulant. Inhibiting Factor Xa diminishes the activation of coagulation and platelets. RXN can be used to minimize the risk of coronary heart disease and embolism individuals with nonvalvular atrial fibrillation, to prevent and/or treat venous thromboembolism, and to treat bioprosthetic mitral valves. It has emerged as an acceptable alternative to vitamin K antagonists, which are more susceptible to drug-drug interactions and more complicated to administer. However, RXN has an inherent risk of bleeding and can increase the risk of hemorrhage when used with other hemostasis-weakening medications. It is not recommended in pregnant or lactating women, children, or those with severe hepatic (ChildPugh C), renal, antiphospholipid syndrome, or artificial heart valves (Kubitza et al., 2010, Patel et al., 2011, Samama et al., 2013, Thomas et al., 2013, Costa et al., 2020, Duarte et al., 2020, Evans et al., 2020, Fernandez et al., 2021, Galiuto and Patrono, 2021). Capell *et al.* discovered that RXN improved the incidence of thrombotic events, hospitalizations, and deaths among symptomatic outpatients with COVID-19 (Capell et al., 2021).

RXN is categorized as a high-permeability and low-solubility substance by the Biopharmaceutical Classification System (BCS) (Class II) (Mueck et al., 2014, Kushwah et al., 2021). It exhibits low pH-independent solubility in aqueous solution. Xarelto is the commercial brand of RXN, and 685–132-2 is the and EC number (European Community) of RXN, respectively (Seshamamba and Sekaran, 2017, Kushwah et al., 2021).

The bioavailability of drugs is limited by their solubility in aqueous media, which is governed by their dissolution time. Reducing the particle size of drugs that are normally water-insoluble is a typical strategy for enhancing their solubility and dissolution rate (Esfandiari, 2015, Esfandiari and Ghoreishi, 2015a,b, Sodeifian et al., 2020a, Esfandiari and Sajadian, 2022a). Supercritical carbon dioxide (SC-CO_2)-based particle production technology is a cutting-edge method for creating nano-sized pharmaceuticals. The rapid mass transfer rate and superior dissolving capability of supercritical fluids can be assigned attributed to

* Corresponding author.
E-mail address: esfandiari_n@miau.ac.ir (N. Esfandiari).

https://doi.org/10.1016/j.arabjc.2024.105707
Received 22 October 2023; Accepted 3 March 2024
Available online 6 March 2024

Nomenclature

a0-a6	Adjustable parameters for density-based models
AARD%	Average absolute relative deviation
C_s	Solute concentration in the collection vial (g/L)
e	Co-solvent enhancement effects
M_{CO2}	CO_2 molecular weight (g/mol)
Ms	Solute molecular weight (g/mol)
M_W	Molecular weight (g/mol)
N	The number of experimental data, dimensionless
n_{CO2}	Mole of CO_2
n_{solute}	Moles of solute (RXN)
P	Pressure (MPa)
Pc	Critical pressure (MPa)
P_{ref}	Reference pressure (0.1 MPa)
Q	The number of self-determining parameters
R^2	Correlation coefficient
R_{adj}	Adjusted correlation coefficient
S	Equilibrium solubility (g/L)
SS_E	Sum square error
SS_T	Total sum of squares
T	Temperature (K)
Tc	Critical temperature (K)
T_m	Melting temperature (K)
y_2	Equilibrium mole fraction
y_2'	Mole fraction in ternary system
y_3	Mole fraction of Co-solvent
V_s	Volume of the collection vial (L)
V_L	Volume of the sampling loop (L)
Z	Number of adjustable parameters

Superscript

Cal	Calculated
Exp	Experimental
i, j	Component

Subscripts

2	Solute
i, j	Component

Abbreviations

ASES	Aerosol solvent extraction system
BCS	Biopharmaceutics Classification System
cEoS	Cubic equations of state
DMSO	Dimethyl sulfoxide
EC number	European Community number
EoS	Equations of State
GAS	Supercritical gas antisolvent
GRAS	Generally Recognized as Safe
GUM	Guide of uncertainty measurement
HBA	Hydrogen-bond acceptor
HBD	Hydrogen-bond donor
HSP	Hansen solubility parameter
KJ	Kumar and Johnston model
KT	Kamlet-Taft solvent parameters
LFHB	Lattice Fluid Hydrogen Bonding
PGSS	Particles from the gas saturated solution
PC-SAFT	Perturbed-chain SAFT
PCP-SAFT	Perturbed-chain polar SAFT
PR	Peng-Robinson
MST	Méndez-Santiago and Teja model
RESS	Rapid expansion of the supercritical solution
RESOLV	Rapid expansion of a supercritical solution into a liquid solvent
RESSAS	Rapid expansion of supercritical solution into aqueous solutions
RV	Retrograde vaporization
RXN	Rivaroxaban
SA	Simulated annealing
SAS	Supercritical antisolvent
SCF	Supercritical fluid
SC-CO_2	Supercritical CO_2
SEDS	Solution-enhanced dispersion by supercritical fluid
SRK	Soave-Redlich-Kowng

Greek symbols

α	H-bond donor
β	H-bond acceptor
π*	Kamlet-Taft dipolarity/polarizability
δ	Hildebrand solubility parameter
λ_{max}	Maxim wave length (nm)
ρ_1	Density of SC-CO_2 (kg m^{-3})
ρ_{ref}	Reference density (700 kg m^{-3})

their viscosities that are more similar to those of gases rather than liquids. Additionally, SC-CO_2 is harmless, colorless, odorless, and leaves no residue in the finished product, further promoting its extensive application in the paramedical industry (Cheng et al., 2018, Ardestani et al., 2020, MacEachern et al., 2020, Pishnamazi et al., 2020a,b, Sodeifian et al., 2020f, Zabihi et al., 2020a, Pishnamazi et al., 2021a). A supercritical fluid (SCF) is frequently used as a dense solvent or anti-solvent to manufacture therapeutic nanoparticles. The solubility of the medicine in the solvent is one of the prerequisites for employing supercritical technology. In general, SCF can be utilized in particle production processes through three different approaches: (i) SCF as a solvent, such as RESS, RESSAS, and RESOLV; (ii) SCF as an anti-solvent, such as GAS, SAS, SEDS, and ASES; and (iii) SCF as a Co-solvent, such as PGSS and PGSS-drying (Esfandiari and Ghoreishi, 2013, Esfandiari and Ghoreishi, 2014, Esfandiari, 2015, Esfandiari and Ghoreishi, 2015a, Cheng et al., 2018, Sodeifian et al., 2019d, MacEachern et al., 2020, Pishnamazi et al., 2020c,b, Najafi et al., 2021, Pishnamazi et al., 2021a, Esfandiari and Sajadian, 2022a).

Throughout the last few decades, the estimation of the solubility of medications in SCFs has become one of the main subjects. So far, a few studies have addressed the reliability and correlation of the solubility documentation of different sorts of medications in SCFs. Table 1 sorts the solubility (crossover and mole fraction points of these medicinal compounds in SC-CO_2) of certain medications examined in the years between 2017 and the present. The solubility of solid components in SCFs offers fundamental facts on the development of small-scale medicinal particles with the ideal size dispersion, to achieve better dissolution rates (Ardestani et al., 2020, Saadati Ardestani et al., 2020, Askarizadeh et al., 2023). Although numerous experimental techniques can evaluate the solubility of a substance, correlations and mathematical

Table 1
Review of some published works on the crossover and mole fraction points of various pharmaceutical compound in SC-CO_2.

Compound	Pressure range (MPa)	Temperature range (K)	Cross over (MPa)	Mole fraction (y)	M_W (g/mol)	Ref
Esomeprazole ($C_{17}H_{19}N_3O_3S$)	12–27	308.2–338.2	22	1.11×10^{-5} to 9.10×10^{-4}	345.42	(Sodeifian et al., 2019b)
Amiodarone hydrochloride ($C_{25}H_{29}I_2NO_3$. HCl)	12–30	313.2–343.2	19	2.510×10^{-5} to 1.012×10^{-3}	681.77	(Sodeifian et al., 2017b)
Ketotifen fumarate ($C_{23}H_{23}NO_5S$)	12–30	308.2–338.2	20	2.11×10^{-5} to 1.07×10^{-3}	425.5	(Sodeifian et al., 2018a)
Aprepitant ($C_{23}H_{21}F_7N_4O_3$)	12–33	308.15–338.15	15–18	4.50×10^{-6} to 7.67×10^{-5}	534.4	(Sodeifian et al., 2017a)
Imatinib mesylate ($C_{30}H_{35}N_7O_4S$)	12–27	308.2–338.2	18–21	1.0×10^{-7} to 4.4×10^{-6}	589.71	(Sodeifian et al., 2019e)
Loratadine ($C_{22}H_{23}N_2O_2Cl$)	12–27	308.15–338.15	18–21	4.50×10^{-6} to 1.30×10^{-3}	382.88	(Sodeifian et al., 2018b)
Loxoprofen ($C_{15}H_{18}O_3$)	12–40	308–338	20	1.04×10^{-5} to 1.28×10^{-3}	246.10	(Zabihi et al., 2020a)
Quetiapine hemifumarate ($C_{21}H_{25}N_3O_2S.0.5C_4H_4O_4$)	12–27	308–338	13–14	0.30×10^{-6} to 9.03×10^{-6}	441.54	(Sodeifian et al., 2021a)
2,4,7-Triamino-6-phenylpteridine (Triamterene) ($C_{13}H_{13}N_7$)	12–27	308–338	19.2–19.5	0.03×10^{-5} to 2.89×10^{-5}	253.26	(Sodeifian et al., 2020a)
Tolmetin ($C_{15}H_{15}NO_3$)	12–40	308–338	16	5.00×10^{-5} to 2.59×10^{-3}	257.29	(Pishnamazi et al., 2020c)
Amlodipine besylate ($C_{26}H_{31}ClN_2O_8S$)	12–27	308–338	NO	4.15×10^{-6} to 23×10^{-6}	567.05	(Sodeifian et al., 2021c)
Busulfan ($C_6H_{14}O_6S_2$)	12–40	308–338	16	3.27×10^{-5} to 8.65×10^{-4}	246.30	(Pishnamazi et al., 2020b)
Sunitinib malate ($C_{26}H_{33}FN_4O_7$)	12–27	308–338	NO	0.5×10^{-5} to 8.56×10^{-5}	532.56	(Sodeifian et al., 2020c)
Fenoprofen ($C_{15}H_{14}O_3$)	12–40	308–338	16	2.01×10^{-5} to 4.20×10^{-3}	242.3	(Zabihi et al., 2020b)
Azathioprine ($C_9H_7N_7O_2S$)	12–27	308–338	12–15	0.27×10^{-5} to 1.83×10^{-5}	277.26	(Sodeifian et al., 2020b)
Sorafenib tosylate ($C_{28}H_{24}ClF_3N_4O_6S$)	12–27	308–338	NO	0.68×10^{-6} to 12.57×10^{-6}	637.03	(Sodeifian et al., 2020d)
Capecitabine ($C_{15}H_{22}FN_3O_6$)	10——35	308.15——348.15	19	3.18×10^{-5} to 120.29×10^{-5}	359.35	(Ardestani et al., 2020)
Aspirin ($C_9H_8O_4$)	10——30	308.15——328.15	13–14	0.33×10^{-4} to 3.45×10^{-4}	180.15	(Ardestani et al., 2020)
Ibuprofen ($C_{13}H_{18}O_2$)	10——30	308.15——333.15	10	0.72×10^{-3} to 3.8×10^{-3}	206.28	(Ardestani et al., 2020)
Repaglinide ($C_{27}H_{36}N_2O_4$)	12–27	308–338	16–18	2.89×10^{-6} to 9.53×10^{-5}	452.29	(Sodeifian et al., 2019d)
Sodium Valproate ($C_8H_{15}NaO_2$)	12–27	308.15——338.15	22–24	0.05×10^{-5} to 3.71×10^{-5}	166.19	(Sodeifian et al., 2020f)
Chloroquine ($C_{18}H_{26}ClN_3$)	12–40	308–338	16–20	1.64×10^{-5} to 8.92×10^{-4}	319.87	(Pishnamazi et al., 2021a)
Decitabine ($C_8H_{12}N_4O_4$)	12–40	308–338	16	2.84×10^{-5} to 1.07×10^{-3}	228.41	(Pishnamazi et al., 2021b)
Oxcarbazepine ($C15_5H_{12}N_2O_2$)	12–27	308–338	17–19	1.10×10^{-7} to 2.675×10^{-5}	252.27	(Sodeifian et al., 2019c)
Sulfabenzamide ($C_{13}H_{12}N_2O_3S$)	12–27	308–338	NO	1.53×10^{-6} to 22.35×10^{-6}	276.3	(Sodeifian et al., 2021d)
Galantamine ($C_{17}H_{21}NO_3$)	12–27	308–338	17–19	0.006×10^{-4} to 0.233×10^{-4}	287.35	(Sodeifian et al., 2021e)
Gliclazide ($C_{15}H_{21}N_3O_3S$)	10–18.6	308.2–328.2	15–17	1.26×10^{-7} to 5.01×10^{-6}	323.41	(Wang et al., 2021)
Captopril ($C_9H_{15}NO_3S$)	10–18.6	308.2–328.2	14–16	3.59×10^{-6} to 9.32×10^{-5}	217.28	(Wang et al., 2021)
Salsalate ($C_{14}H_{10}O_5$)	12–40	308–338	16	3.77×10^{-5} to 3.88×10^{-3}	258.23	(Zabihi et al., 2021a)
Lansoprazole ($C_{16}H_{14}F_3N_3O_2S$)	12–27	308.2–338.2	21	1.15×10^{-5} to 7.36×10^{-4}	369.36	(Sodeifian et al., 2020g)
(Letrozole) ($C_{17}H_{11}N_5$)	12–36	318.2–348.2	16–18	1.6×10^{-6} to 8.51×10^{-5}	263.33	(Sodeifian and Sajadian, 2018)
Rivaroxaban ($C_{19}H_{18}ClN_3O_5S$)	12–27	308–338	22.5	0.0104×10^{-4} to 0.2062×10^{-2}	435.90	(Sodeifian et al., 2023e)
Tamsulosin ($C_{20}H_{28}N_2O_5S$)	12–27	308–338	21	0.18×10^{-6} to 1.013×10^{-5}	408.05	(Hazaveie et al., 2020)
Gambogic acid ($C_{38}H_{44}O_8$)	10–30	308.15–328.15	20	1.63×10^{-6} to 22.62×10^{-6}	628.76	(Xiang et al., 2019)
Tamoxifen ($C_{26}H_{29}NO$)	12–40	308–338	20	1.88×10^{-5} to 9.89×10^{-4}	371.51	(Pishnamazi et al., 2020a)
Losartan potassium, Cozaar ($C_{22}H_{22}ClN_6O$)	12–27	308–338	19	2.03×10^{-6} to 1.88×10^{-5}	461	(Sodeifian et al., 2021f)

(*continued on next page*)

Table 1 (*continued*)

Compound	Pressure range (MPa)	Temperature range (K)	Cross over (MPa)	Mole fraction (y)	M_W (g/mol)	Ref
Gatifloxacin ($C_{38}H_{50}F_2N_6O_{11}$)	12–36	313–333	14	0.106×10^{-6} to 1.605×10^{-6}	375.4	(Shi et al., 2017, Padrela et al., 2018)
Enrofloxacin ($C_{19}H_{22}FN_3O_3$)	17–36	313–333	17	0.022×10^{-6} to 5.605×10^{-6}	359.4	(Shi et al., 2017, Padrela et al., 2018)
Ciprofloxacin ($C_{17}H_{19}ClFN_3O_3$)	24–36	313–333	NO	0.0265×10^{-6} to 0.1887×10^{-6}	331.34	(Shi et al., 2017, Padrela et al., 2018)
Penicillin G (Benzylpenicillin) ($C_{16}H_{18}N_2O_4S$)	10–35	313.15–333.35	10	0.420×10^{-5} to 6.330×10^{-5}	334.4	(Gordillo et al., 1999, Padrela et al., 2018)
Lenalidomide ($C_{13}H_{13}N_3O_3$)	12–30	308–338	18	0.02×10^{-4} to 1.08×10^{-4}	259.25	(Sajadian et al., 2022a)
Glibenclamide ($C_{23}H_{28}ClN_3O_5S$)	12–30	308–338	21	0.8×10^{-6} to 8.03×10^{-5}	494	Esfandiari and Sajadian, 2022b
Montelukast ($C_{35}H_{36}ClNO_3S$)	12–30	308–338	15	0.4×10^{-6} to 6.12×10^{-5}	586.18	(Sajadian et al., 2022c)
Minoxidil ($C_9H_{15}N_5O$)	12–27	308–338	19	0.24×10^{-6} to 3.39×10^{-6}	209.25	(Sodeifian et al., 2020e)
Ketoconazole ($C_{26}H_{28}C_{l2}N_4O_4$)	12–30	308–338	13–15	0.20×10^{-6} to 8.02×10^{-4}	531	(Sodeifian et al., 2021g)
Sertraline. HCl ($C_{17}H_{17}C_{l2}N$. HCl)	12–30	308–338	17–19	0.61×10^{-4} to 0.89×10^{-3}	342.69	(Sodeifian et al., 2019)
Favipiravir ($C5H_4FN_3O_2$)	12–30	308–338	18	3.0×10^{-6} to 9.05×10^{-4}	157.1	(Sajadian et al., 2022b)
Dasatinib Monohydrate ($C_{22}H_{28}ClN_7O_3S$)	12–27	308–338	NO	0.45×10^{-6} to 9.08×10^{-6}	505.16	(Sodeifian et al., 2022h)
Clemastine Fumarate ($C_{21}H_{26}ClNO{\cdot}C_4H_4O_4$)	12–27	308–338	NO	1.61×10^{-6} to 9.41×10^{-6}	460	(Sodeifian et al., 2021b)
Teriflunomide ($C_{12}H_9F_3N_2O_2$)	12–27	308–338	19.5	8.84×10^{-5} to 5.43×10^{-4}	270.21	(Sodeifian et al., 2022g)
Metoclopramide hydrochloride ($C_{14}H_{23}C_{l2}N_3O_2$)	12–27	308–338	22	0.15×10^{-5} to 5.56×10^{-5}	336.26	(Sodeifian et al., 2022f)
Pholcodine ($C_{23}H_{30}N_2O_4$)	12–27	308–338	16–16.5	2.06×10^{-4} to 5.93×10^{-4}	398.55	(Sodeifian et al., 2022a)
Lacosamide ($C_{13}H_{18}N_2O_3$)	12–30	308–338	12–18	1×10^{-6} to 2.29×10^{-4}	250.3	(Esfandiari and Ali Sajadian, 2022)
Febuxostat ($C_{16}H_{16}N_2O_3S$)	12–27	308–338	21	0.05×10^{-4} to 7.42×10^{-4}	316.37	Abourehab et al., 2022b; Zabihi et al., 2021b
Paracetamol ($C_8H_9NO_2$)	9.5–26.5	311–358	11	0.305×10^{-6} to 16.358×10^{-6}	151.16	(Bagheri et al., 2022)
Methylparaben ($C_8H_8O_3$)	12–35.5	308–348	15.2	1.13×10^{-5} to 1.213×10^{-3}	152.16	(Mahesh and Garlapati, 2022)
Ethylparaben ($C_9H_{10}O_3$)	8–21	308–328	8	1.64×10^{-6} to 1.755×10^{-5}	166.17	(Mahesh and Garlapati, 2022)
Propylparaben ($C_{10}H_{12}O_3$)	9.41–22.02	308.15—328.15	14	4.4×10^{-6} to 6.12×10^{-5}	180.2	(Mahesh and Garlapati, 2022)
Empagliflozin ($C_{23}H_{27}ClO_7$)	12–27	308–338	16.5	5.14×10^{-6} to 25.9×10^{-6}	450.91	(Sodeifian et al., 2022c)
Pantoprazole sodium sesquihydrate ($C_{16}H_{14}F_2N_3NaO_4S \times 1.5\ H_2O$)	12–27	308–338	16	0.0301×10^{-4} to 0.463×10^{-4}	432.4	(Sodeifian et al., 2022d)
Prazosin hydrochloride ($C_{19}H_{22}ClN_5O_4$)	12–27	308–338	NO	1.59×10^{-5} to 7.2×10^{-5}	419.9	(Sodeifian et al., 2022i)
Temozolomide ($C_6H_6N_6O_2$)	12–40	308–338	20	4.30×10^{-4} to 5.28×10^{-3}	194.1	(Zabihi et al., 2021b)
Cefuroxime axetil ($C_{20}H_{22}N_4O_{10}S$)	8–25	308–328	Higher than 25 MPa	2.2×10^{-7} to 11.24×10^{-6}	510.47	(Ongkasin et al., 2019)
Ethosuximide ($C_7H_{11}NO_2$)	9–15	313.15–328.15	NO	3.45×10^{-3} to 8.71×10^{-3}	141.168	(Zha et al., 2019)
(Octatrimethylsiloxy) Polyhedral oligomeric silsesquioxanes (POSS) $C_{24}H_{72}OO_{20}Si_{16}$	1–30	308–328	10.6	0.0083 to 2×10^{-3}	1146.18	(Demirtas and Dilek, 2019)
Chlorothiazide ($C_7H_6ClN_3O_4S_2$)	13–29	308–338	17	0.417×10^{-5} to 1.012×10^{-5}	295.73	(Majrashi et al., 2023)
Pazopanib hydrochloride ($C_{21}H_{24}ClN_7O_2S$)	12–27	308–338	NO	1.87×10^{-6} to 14.25×10^{-6}	474	(Sodeifian et al., 2022b)
Crizotinib ($C_{21}H_{22}Cl_2FN_5O$)	12–27	308–338	14.5	0.156×10^{-5} to 1.219×10^{-5}	450.3	(Sodeifian et al., 2022e)
Alendronate ($C_4H_{13}NO_7P_2$)	12–30	308–338	18	0.01×10^{-4} to 1.5×10^{-4}	271.08	Abourehab et al., 2022a
Sildenafil citrate ($C_{22}H_{30}N_6O_4S$)	12–30	308–338	15–18	2.40×10^{-7} to 6.48×10^{-6}	474.6	(Honarvar et al., 2023)
Riluzole ($C_8H_5F_3N_2OS$)	12–27	308–338	22	4.95×10^{-5} to 1.49×10^{-4}	234.2	(Abadian et al., 2022)
Fludrocortisone acetate ($C_{23}H_{31}FO_6$)	12–30	308–338	18–21	0.211×10^{-6} to 0.653×10^{-5}	422.5	(Amani et al., 2022)
Metformin ($C_4H_{11}N_5$)	14–29	308–328	NO	0.39×10^{-6} to 1.23×10^{-6}	129.16	(Venkatesan et al., 2022)

(*continued on next page*)

Table 1 (*continued*)

Compound	Pressure range (MPa)	Temperature range (K)	Cross over (MPa)	Mole fraction (y)	M_W (g/mol)	Ref
Haloperidol ($C_{21}H_{23}ClFNO_2$)	12–22	313.2–323.2	17–19	3.4×10^{-7} to 1.4×10^{-5}	375.9	(Khudaida et al., 2023a)
Retinol Vitamin A ($C_{20}H_{3O}$)	9–23.3	303–323	11	2.18×10^{-5} to 1.964×10^{-4}	286.45	(Naikoo et al., 2021)
Famotidine (FAM) ($C_8H_{15}N_7O_2S_3$)	12–30	308–338	18	1.4×10^{-6} to 1.11×10^{-4}	337.43	(Saadati Ardestani et al., 2023)
Erlotinib hydrochloride ($C_{22}H_{24}N_3O_4Cl$)	12–30	308–338	19–22	1.2×10^{-6} to 2.12×10^{-5}	429.9	(Bazaei et al., 2023)
Phemytoin ($C_{15}H_{12}N_2O_2$)	9.5–25	313–345	11	0.68×10^{-6} to 15.7×10^{-6}	252.268	(Notej et al., 2023)
Raloxifene ($C_{28}H_{27}NO_4S$)	9.5–25	313–345	12	0.79×10^{-5} to 8.09×10^{-5}	473.59	(Notej et al., 2023)
Clonazepam ($C_{15}H_{10}ClN_3O_3$)	12–30	308–338	20	3.9×10^{-6} to 7.26×10^{-5}	315.71	(Alwi et al., 2023)
Curcumin (C21H20O6)	8–20	308.15–328.15	13	1.82×10^{-8} to 1.97×10^{-6}	368.38	(Zhan et al., 2017)
Dibutylbutyl phosphonate ($C_{12}H_{27}O_3P$)	10–25	313–333	11	0.087 to 0.117	250.31	(Pitchaiah et al., 2017)
Diamylamyl phosphonate ($C_{15}H_{33}O_3P$)	10–25	313–333	12	0.065 to 0.09	292.4	(Pitchaiah et al., 2017)
Ipriflavone ($C_{18}H_{16}O_3$)	10–20	308.2–328.2	15	1.4×10^{-4} to 2.2×10^{-4}	280.3	(Wang and Su, 2020)
Tolbutamide ($C_{12}H_{18}N_2O_3S$)	10–30	313.15–353.15	17–20	1.66×10^{-5} to 40.5	270.35	(Manna and Banchero, 2018)
Chlorpropamide ($C_{10}H_{13}N_2O_3S$)	10–30	313.15–353.15	17–20	2.29×10^{-6} to 72.2×10^{-6}	276.74	(Manna and Banchero, 2018)
1-aminoanthraquinone ($C_{14}H_9NO_2$)	12.5–25	323.15–383.15	17	5.5×10^{-7} to 351×10^{-7}	223.23	(Tamura et al., 2017)
1-nitroanthraquinone ($C_{14}H_7NO$)	12.5–25	323.15–383.15	18–20	9.8×10^{-7} to 252.3×10^{-7}	253.21	(Tamura et al., 2017)
Phthalocyanines green (Pc-G)	10–35	308.15–338.15	22	0.01×10^{-5} to 12.12×10^{-5}	1127.154	(Sodeifian et al., 2019f)
Fampridine (pyridin-4-amine, 4-aminopyridine) ($C_5H_6N_2$)	10–22	308.2–328.2	10.5–12.5	2×10^{-5} to 2×10^{-4}	94.11	(Chen et al., 2017)
Vitamin E acetate (α-tocopheryl acetate) (VEA) ($C_{31}H_{52}O_3$)	8–15	308.15–328.15	NO	2.76×10^{-4} to 7.26×10^{-4}	472.76	(Han et al., 2017)
Anthraquinone violet 3RN (AV3RN) ($C_{28}H_{20}N_2Na_2O_8S_2$)	10–34	308–338	10	0.047×10^{-5} to 0.546×10^{-5}	622.58	(Saadati Ardestani et al., 2020)
Phosphatidylcholine (PC) ($C_{42}H_{80}NO_8P$)	12.4–17.2	313–353	NO	5.082×10^{-6} to 11.758×10^{-6}	758.1	(Jash et al., 2020)
Coumarin-7 ($C_{20}H_{19}N_3O_2$)	9–33	308–338	13–16	0.415×10^{-5} to 1.009×10^{-5}	333.38	(Sodeifian et al., 2019a)
Vanillin ($C_8H_8O_3$)	8–28	313–353	16	0.14×10^{-3} to 13×10^{-3}	152.15	(Maqbool et al., 2017)
Phenol (C_6H_6O)	10–35	333–363	28	1.14×10^{-3} to 9.064×10^{-2}	94.11	(Maqbool et al., 2017)
Flufenamic acid (FFA ($C1_4H_{10}F_3NO_2$)	8–21	313.2–333.2	14	0.8×10^{-6} to 2.13×10^{-4}	281.23	(Tsai et al., 2017)
Nystatin ($C_{47}H_{75}NO_{17}$)	12–30	308–338	22	0.40×10^{-6} to 1.20×10^{-5}	926.1	(Sajadian et al., 2023)
Aripiprazole ($C_{23}H_{27}CL_2N_3O_2$)	12–30	308–338	18	1.83×10^{-6} to 1.036×10^{-5}	448.39	(Ansari et al., 2023)
Nifedipine ($C_{17}H_{18}N_2O_6$)	12.5–27.5	333.15–353.15	18	7.9×10^{-6} to 53.6×10^{-6}	346.3	(Li et al., 2017)
Quinine ($C_{20}H_{24}N_2O_2$)	12.5–27.5	323.15–343.15	15–19	12×10^{-6} to 50.4×10^{-6}	324.4	(Li et al., 2017)
Nilotinib hydrochloride monohydrate ($C_{28}H_{25}ClF_3N_7O_2$)	12–27	308–338	12–15	0.1×10^{-5} to 0.59×10^{-5}	584	(Nateghi et al., 2023)
Palbociclib ($C_{24}H_{29}N_7O_2$)	12–27	308–338	12–15	0.081×10^{-5} to 2.027×10^{-5}	447.533	(Sodeifian et al., 2023c)
Oxaprozin ($C_{18}H_{15}NO_3$)	12–40	308–338	NO MEN	3.31×10^{-5} to 1.24×10^{-3}	293.317	(Alshehri et al., 2022)
lutein (β,ε-carotene-3,3′-diol) ($C_{40}H_{56}O_2$)	18.7–33.55	313–333	NO	0.82×10^{-6} to 2.45×10^{-6}	568.89	(Araus et al., 2019)
Metoprolol ($C_{15}H_{25}NO_3$)	12–30	308–338	18	$0.02 \times 10^{-5}$to 8.11×10^{-5}	267.36	(Alshahrani et al., 2023)
Chlorpromazine ($C_{17}H_{19}ClN_2S$)	17–41	308–348	20	$3.21 \times 10^{-5}$to 5.25×10^{-5}	318.9	(Alharby et al., 2023)
Hyoscine ($C_{17}H_{21}NO_4$)	17–40	308–348	20	$0.79 \times 10^{-4}$to 2.83×10^{-4}	303.3	(Hani et al., 2023)
Verapamil ($C_{27}H_{38}N_2O_4$)	12–30	308–338	12–15	$3.6 \times 10^{-6}$to 7.14×10^{-5}		(Esfandiari et al., 2023)
Buprenorphine hydrochloride ($C_{29}H_{42}ClNO_4$)	12–27	308–338	15–18	$0.131 \times 10^{-4}$to 4.752×10^{-4}	504.1	(Sodeifian et al., 2023a)
Hydroxychloroquine sulfate ($C_{18}H_{28}ClN_3O_5S$)	12–27	308–338	NO	0.0304×10^{-5} to 0.5515×10^{-5}	434	(Sodeifian et al., 2023b)

(*continued on next page*)

Table 1 (*continued*)

Compound	Pressure range (MPa)	Temperature range (K)	Cross over (MPa)	Mole fraction (y)	M_W (g/mol)	Ref
Probenecid ($C_{13}H_{19}NO_4S$)	15–21	313.2–353.2	15–19	$0.13 \times 10^{-5}$to 1.45×10^{-5}	285.36	(Khudaida et al., 2023b)
Warfarin ($C_{19}H_{16}O_4$)	10–18	308.2–328.2	18	1.48×10^{-6} to 4.32×10^{-6}	434	(Ciou et al., 2018)
Ibrutinib ($C_{25}H_{24}N_6O_2$)	12–27	308–338	17	3.90×10^{-6} to 1.30×10^{-5}	440.51	(Sodeifian et al., 2023d)
Sitagliptin phosphate ($C_{16}H_{18}F_6N_5O_5P$)	12–30	308–338	15–16.5	3.02×10^{-5} to 6.98×10^{-5}	407.31	(Ardestani et al., 2023)

NO: In the pressure range, the crossover is not exit.
NO MEN: In the article, the crossover is not calculated.

Table 2
The sources and purity of the materials used in this work.

Material	Source	Initial mass fraction (Purity)	Final mass fraction Purity	Analysis method
Rivaroxaban	Tofigh Daru Research & Engineering Co.	0.99	0.99	HPLC[a]
Ethanol	Merck Co.	0.999	0.999	GC[b]
Carbon dioxide	Novin Oxygen Co.	0.9999	0.9999	GC

[a] High-performance liquid chromatography.
[b] Gas chromatography.

models are frequently implemented to estimate the solubility of the substances in SC-CO_2 due to the high cost of experimental measurements. In general, semi-empirical models and equation of state (EoS)-based models can be used to correlate the solubility data. EoS-based models require complex computational techniques and data for a variety of physical variables (cubic equations of state (Peng-Robinson (PR) (Peng and Robinson, 1976) and Soave-Redlich-Kowng (SRK) (Soave, 1972)) or perturbation equations (perturbed-chain polar SAFT (PCP-SAFT) (Gross, 2005), PC-SAFT (Gross and Sadowski, 2001))). Semi-empirical equations, like density-based models, only require easily accessible control items i.e., temperature, pressure, and the density of CO_2 with no need for thermophysical properties such as molar volume, acentric factor, and critical point, which cannot be estimated (Sodeifian et al., 2019e, Ardestani et al., 2020, Zhan et al., 2020, Zabihi et al., 2021a). Numerous semi-empirical models have been geared towards connecting the solubility data of solids in SC-CO_2; among which, Kumar and Johnston (KJ) (Kumar and Johnston, 1988), Bartle *et al.* (Bartle et al., 1991), Khansary *et al.* (Khansary et al., 2015), Jouyban *et al.* (Jouyban et al., 2002b), Chrastil (Chrastil, 1982), Adachi-Lu (Adachi and Lu, 1983), Garlapati – Madras (Garlapati and Madras, 2010), González *et al.* (González et al., 2001), Mendez – Santiago – Teja (MST) (Sauceau et al., 2003), Li *et al.* (Li et al., 2003), Soltani – Mazloumi (Soltani and Mazloumi, 2017), Reddy – Madras (Reddy and Madras, 2011), Keshmiri *et al.* (Keshmiri et al., 2014), Bian *et al.* (Bian et al., 2011), Sodeifian *et al.* (Sodeifian et al., 2019), Sparks *et al.* (Sparks et al., 2008), Del Valle and Aguilera (Del Valle and Aguilera, 1988), Tan (Yeoh et al., 2013), Gordillo (Gordillo et al., 1999), Yu (Yu et al., 1994), Sung and Shim (Sung and Shim, 1999) can be mentioned.

One of the biggest challenges in the development of the SCF process is the limited solubility of polar solutes in SC-CO_2. As the majority of pharmaceuticals are polar molecules, the interaction of carbon dioxide (a nonpolar structure) with medications is limited. Therefore, supercritical CO_2 is employed in combination with other solvents, known as "Co-solvent", to enhance the solubility. Co-solvents can alter the polarity of the solvent. Consequently, the use of Co-solvents can enhance the solubility in SCFs (polar or non-polar). Moreover, the incorporation of small amounts (less than 10 %) of polar solvents, such as acetone, dimethyl sulfoxide (DMSO), ethanol, menthol, and methanol can significantly increase the solute solubility in SC-CO_2 (Hosseini et al., 2018, Bitencourt et al., 2019, Ardestani et al., 2020, Saadati Ardestani et al., 2020, Sodeifian et al., 2021g). These Co-solvents can participate in hydrogen bonding with solute molecules and increase the solvation power of a specific supercritical fluid in solvents with lower solvation ability like water. Additionally, the impact of the Co-solvent is related to an improvement in solubility by a rise in solvent density or by intermolecular cooperation between the Co-solvent and the solute. Furthermore, an increase in the specific intermolecular interactions between the Co-solvent and one or more components of the mixed components can enhance the separation selectivity (Knez et al., 2017, Bitencourt et al., 2019, Saadati Ardestani et al., 2020, Zhan et al., 2020).

The Co-solvent effect is primarily influenced by heightened intermolecular interactions and solvent density. In systems with multiple components, solubility can be significantly increased, but selectivity remains unaffected if the increase is solely due to higher solvent mixture density. The density input to the Co-solvent impact is affected by pressure, temperature, and the addition of a Co-solvent, which can lead to the formation of clusters of SCF molecules around it, boosting overall density. The greatest density increase is observed near the critical point of the solvent mixture. An increase in pressure decreases clustering, increases SCF density, and decreases density differences between the

Table 3
Properties of Rivaroxaban (M_w: Molar mass, T_m: melting point, λ_{max}: λ with maximum absorbance).

Component	Formula	M_w (g/mol)	T_m (K)	λ_{max} [nm]	Structure	CAS number
Rivaroxaban	$\mathbf{C_{19}H_{18}ClN_3O_5S}$	435.88	503.15	249	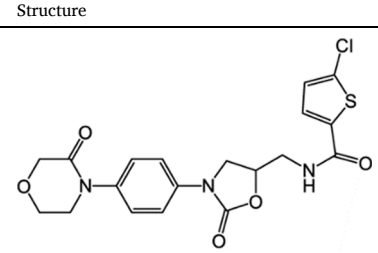	366789–02-8

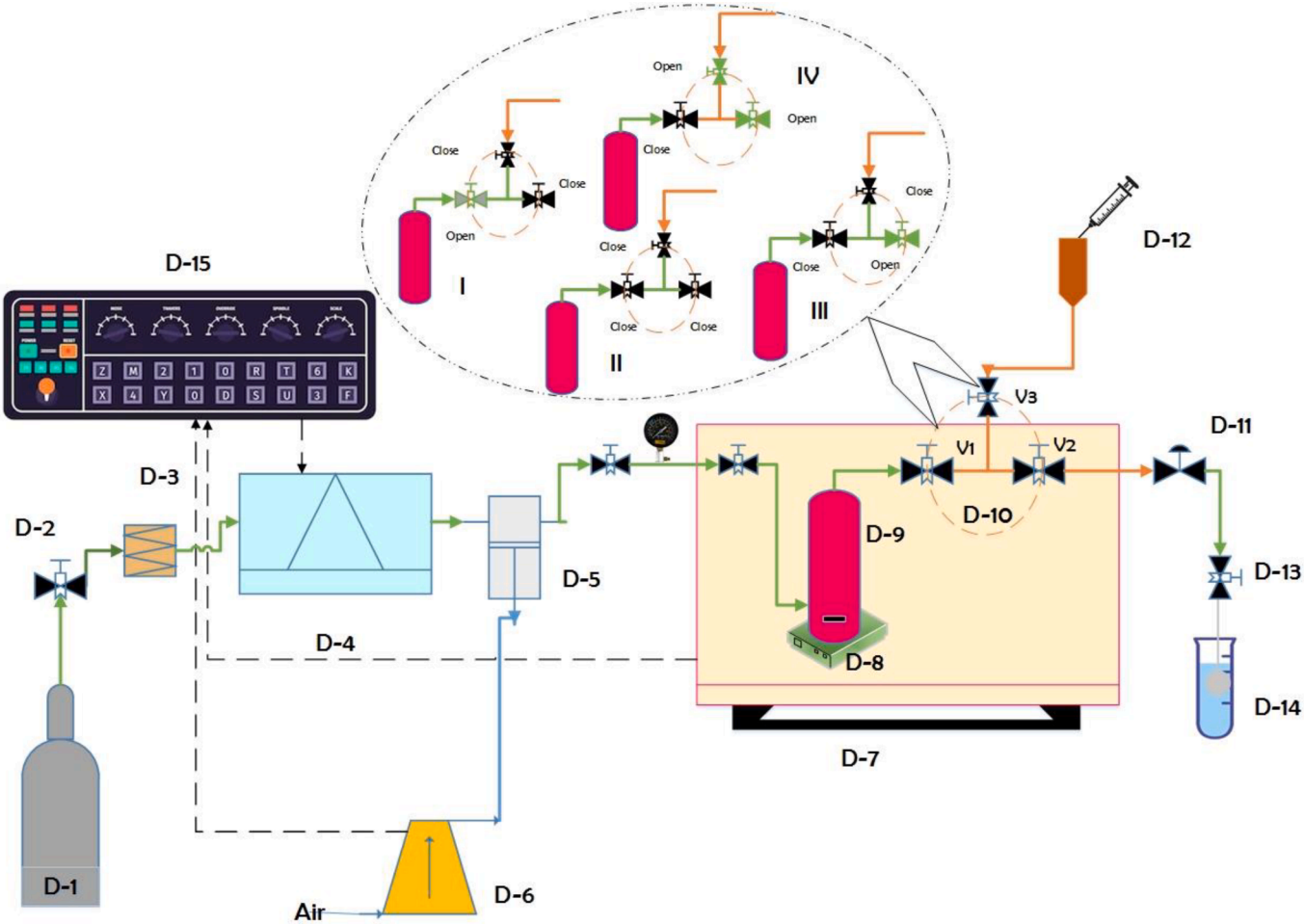

	Description
D-1	CO_2 Tank
D-2	Needle valve
D-3	Filter
D-4	Refrigerator unit
D-5	High pressure pump (Haskel pump)
D-6	Compressor
D-7	Oven
D-8	Magnetic stirrer
D-9	Equilibrium cell
D-10	Loop
D-11	Back-pressure valve
D-12	Syringe
D-13	Metering valve
D-14	Collection vial
D-15	Control panel

Fig. 1. Schematic diagram of experimental apparatus used for measuring solubility.

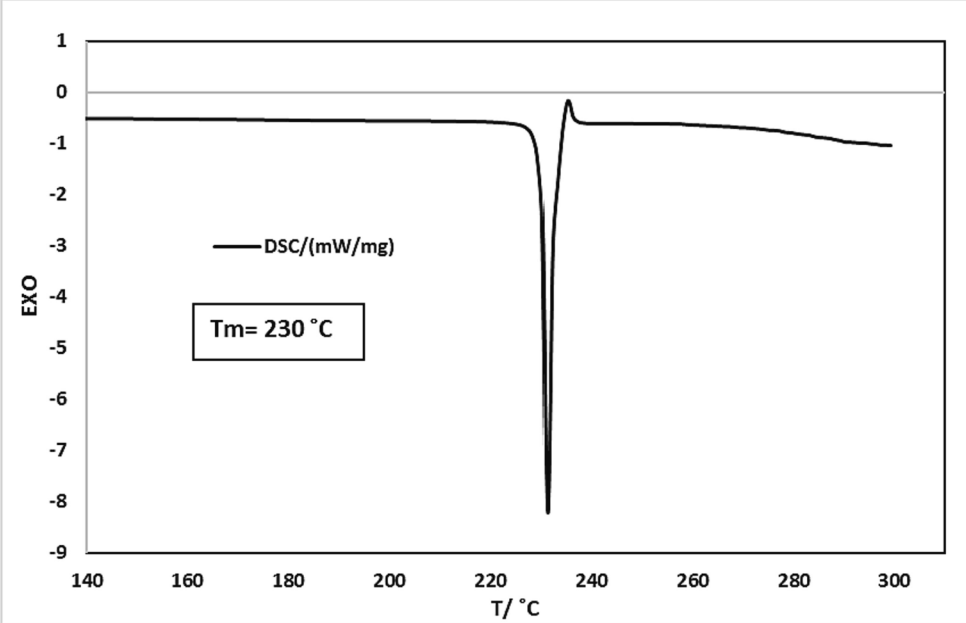

Fig. 2. DSC analysis of Rivaroxaban.

SCF and SCF mixture, ultimately crossing density isotherms. The addition of a Co-solvent can strengthen the SCF solvent while decreasing the molar density of the solvent. Key factors influencing the Co-solvent effect include various physical interactions like dipole-induced dipole, dipole–dipole, and induced dipole-induced dipole (dispersion), as well as specific interactions like charge transfer and H-bonding complexes. A comprehensive understanding of the Co-solvent effect requires a thorough comprehension of intermolecular interactions between solvents and solutes (Prausnitz et al., 1999, Güçlü-Üstündağ and Temelli, 2005, Cui et al., 2018, Li et al., 2018, Pitchaiah et al., 2018, Peyrovedin and Shariati, 2020, Matin et al., 2022, Sajadian et al., 2023).

The Hildebrand solubility parameter (δ) and the Hansen solubility parameter (HSP) are commonly used to assess suitable solvents for specific applications based on similar solubility parameters. HSP categorizes molecular interactions into dispersion, hydrogen-bond, and polar contributions, making it applicable to both polar and non-polar mixtures. Kamlet-Taft solvent parameters (KT) like α (H-bond donor) (HBD), β (H-bond acceptor) (HBA), and solvent dipolarity/polarizability (π^*) help evaluate total solvent polarity. The entertainer effect enhances selectivity and solubility through specific intermolecular interactions like H-bonding between Co-solvent and solutes. When selecting a binary mixed-solvent, the one with higher KT-acidity is the HBD solvent, and the local composition of the HBD-HBA pair influences KT-parameters of complex molecules. In SC-CO_2, non-aqueous and aqueous HBD-HBA solvent pairs act as Co-solvents, interacting with polar solutes and CO_2. The HBD-HBA complex molecule impacts selectivity by specific interactions with solutes and CO_2 affinity (CO_2 philicity). Adjusting the HBD-HBA Co-solvent composition can enhance basicity, CO_2 philicity, and specific interactions for solute dissolution in the SC-CO_2 phase (Güçlü-Üstündağ and Temelli, 2005, Cui et al., 2018, Duereh and Smith, 2018, Li et al., 2018, Pitchaiah et al., 2018).

This research is aimed at understanding the solubility of RXN in SC-CO_2 with or without ethanol as a Co-solvent. The static equilibrium test conditions involve the pressure range of 12, 15, 17, 21, 24, 27 and 30 MPa and temperatures of 308, 318, 328, and 338 K. The solubility of RXN in SC-CO_2 was experimentally studied to investigate the impacts of the operational factors such as temperature, pressure, and the presence of a Co-solvent. The density models of Jouyban *et al.*, Soltani-Mazloumi, Méndez-Santiago-Teja (MST), Sodeifian-Sajadian, González *et al.*, Garlapati–Madras, Chrastil, Kumar and Johnston (KJ), Bian *et al.* and Bartle *et al.* were used to correlate the solubility data of RXN in binary and ternary procedures. The model parameters were established, and the average absolute relative deviation (AARD (%)) was also utilized to evaluate the prediction effectiveness of the method.

2. Experiments

2.1. Materials

Rivaroxaban was acquired from Tofigh Darou drug company (Tehran, Iran) with a purity of 99 %. Additionally, further information regarding other components including carbon dioxide and ethanol can be found in Table 2. The structure of Rivaroxaban is provided in Table 3.

2.2. Experimental apparatus

Based on Fig. 1, the experimental pilot plant was equipped with a spectrophotometer and included a CO_2 tank, an air compressor (Finac, China), a high-pressure pump (Haskel pump, Burbank CA 91502, USA), a refrigeration machine, a magnetic stirrer with 100 rpm, a filter, flow control valves like a needle valve, a back-pressure valve, a metering valve, an equilibrium cell, and an oven (Memert, Germany). All the components of this high-pressure unit, including the pipeline and fittings, have a diameter of 1/8 in. and are made of 316 stainless steel. The impurities in the CO_2 flow from the tank were eliminated by passing through a molecular filter with a pore size of 1 μm. The flow then reached the cooling unit where the CO_2 flow liquefied due to the low interior temperature of the refrigerator (~-15 °C). From the pressure of

Table 4
A summary of the binary semi-empirical and empirical models used in this work Table 4. b Summary of the Ternary semi-empirical and empirical models used in this work.

Model	Formula/ explain	constant	ref
Chrastil Semi-empirical	$lny_2 = a_0 + a_1 ln\rho_1 + \frac{a_2}{T}$ An equation describes the formation of a solvate complex AB_k in a system where one unit of solute A combines with k units of solvent B. It highlights a correlation between solubility and density in a supercritical fluid, as well as a relationship between solubility and temperature. However, Chrastil's equation has limitations, such as being unsuitable for solubility levels above 100–200 kg m^{-3} and lacking validity across a wide range of temperatures. This model is designed for pure fluids and can be applied in mixtures with consistent Co-solvent mole fractions, assuming these mixtures behave like pure fluids at constant concentrations. Overall, the model provides a macroscopic view of the molecular environment in the fluid phase without requiring knowledge of the solute's properties.	3	(Chrastil, 1982) (Sauceau et al., 2003, Hojjati et al., 2007, Sparks et al., 2008, Kostrzewa et al., 2019)
Bartle *et al.* Semi-empirical	$ln\left(\frac{y_2P}{P_{ref}}\right) = a_0 + \frac{a_1}{T} + a_2(\rho_1 - \rho_{ref})$ This model illustrates the relationship between solubility and solvent density. The correlation is expressed in a linear manner using the enhancement factor of the solute with respect to the density of the solvent. By fitting the correlation to experimental data, the coefficients a_0, a_1, and a_2 can be determined. The parameter a_2 is particularly useful in estimating the heat of vaporization of the solute, H_{vap} ($H_{vap} = -a_2R$). By utilizing the values of H_{total} and H_{vap}, the heat of solvation can be estimated for each solute-CO_2 system. The Bartle model, which includes an individual pressure term, is expected to provide more reliable correlated results for solubility data at different pressures.	3	(Bartle et al., 1991) (Hojjati et al., 2007, Sparks et al., 2008)
Mendez − Santiago − Teja (MST) Semi-empirical	$Tln(y_2P) = a_0 + a_1\rho_1 + a_2T$ This model utilizes the principles of dilute solutions and employs the algorithm of the Henry constant of solute in a supercritical fluid. Within this theoretical framework, the enhancement factor is ascertained by the solvent's density, leading to straightforward equations for a range of thermodynamic properties of dilute near-critical binary mixtures. Additionally, this model allows for the normalization of data across varying temperatures.	3	(Sodeifian et al., 2018a) (Sauceau et al., 2003, Hojjati et al., 2007, Sparks et al., 2008)
Jouyban *et al.* Empirical	$lny_2 = a_0 + a_1P + a_2P^2 + a_3PT + \frac{a_4T}{P} + a_5\ln(\rho_1)$ The solubilities of organic solids in SC-CO_2 can be accurately predicted using the empirical model developed by Jouyban *et al.* This model takes into account the interplay between solute mole fraction, linear pressure, and temperature, allowing for the estimation of solubility data that has not been measured. Additionally, it can be used to identify any outliers in experimental solubility data, providing valuable insights into the behavior of these systems.	6	(Jouyban et al., 2002a, 2002b) (Jouyban et al., 2002a, Sridar et al., 2013)
Bian *et al.* Empirical	$y_2 = \rho_1^{a_0+a_1\rho} exp\left(\frac{a_2 + a_3\rho_1}{T} + a_4\right)$ The density-based empirical model proposed by Bian *et al.* offers a comprehensive understanding of the solubility of compounds in SC-CO_2. It accounts for the intricate interplay between solubility and density of the supercritical fluid at varying temperatures and pressures. Additionally, it considers the correlation between solubility and temperature under isopycnic conditions, as well as the impact of temperature and pressure on the association number. This model is derived from Chrastil's equation.	5	(Bian et al., 2011) (Sridar et al., 2013)
Kumar and Johnston (KJ) Semi-empirical	$lny_2 = a_0 + a_1\rho_1 + \frac{a_2}{T}$ In 1988, a thermodynamic formalism was introduced to explain the connection between the solubility of a nonvolatile solute in a SCF and the density of the fluid phase. This model suggests that the logarithm of the solute's mole fraction in the fluid phase shows a nearly linear relationship with either the logarithm or the density of the SCF phase in the vicinity of the critical point, depending on the specific system. The slope of this linear correlation is determined by both the partial molar volume of the solute in the SCF phase and the isothermal compressibility of the fluid. Through the analysis of solubility data from existing literature, scientists have been able to calculate partial molar volumes using this framework, and these calculated values are in good agreement with independently measured data.	3	(Kumar and Johnston, 1988) (Kumar and Johnston, 1988, Yan et al., 2022)

Model	Formula	constant	Ref
Mendez−Santiago−Teja (MST) semi-empirical	$Tln\left(\frac{y_2'P}{P_{ref}}\right) = a_0 + a_1\rho_1 + a_2T + a_3y_3$ A correlation with four adjustable parameters was derived by combining the Mendez-Santiago and Teja equation with a Clausius-Clapeyron-type equation and including sublimation pressure. This correlation is used to assess the impact of density, temperature, and Co-solvent composition on the solubility of the ternary system.	4	(Méndez-Santiago and Teja, 1999) (Sauceau et al., 2003)
Sodeifian-Sajadian semi-empirical	$ln(y_2') = (a_0 + \frac{a_1\rho_1}{T})ln(\rho_1) + a_2\rho_1 + a_3ln(y_3P)$ Four experimental data points were selected as the minimum requirement from the collected data sets to train the proposed model for determining the solubilities of organic solids in SC-CO_2 when a Co-solvent is present. The development of this model is based on the works of González et al. and Chrastil models.	4	(Sodeifian et al., 2019c) (Rojas et al., 2023)
González *et al.* semi-empirical	$ln(y_2') = a_0ln(\rho_1) + a_1ln(y_3) + \frac{a_2}{T} + a_3$ González and colleagues introduced a thermodynamic model based on the Chrastil model, utilizing the mass-action law to predict solute solubility in non-entrained supercritical fluids. This model has shown effectiveness, especially in systems where the presence of an entrainer boosts solute solubility significantly, particularly in cases with strong solute-entrainer interaction. The model incorporates the logarithmic dependence of solubility on fluid density along with an exponential relationship between solubility and Co-solvent concentration. It is built on the assumption of cluster or solvate complex formation involving the solute, entrainer, and solvent, which is consistent with the observed decrease in solute solubility with	4	(González et al., 2001) (González et al., 2001)

(*continued on next page*)

Table 4 (*continued*)

Model	Formula	constant	Ref
	temperature. Therefore, the model may not accurately forecast solubility in systems where the Co-solvent only serves as a Co-solvent for CO_2, lacking the entrainer effect that enhances both solubility and extraction selectivity.		
Soltani-Mazloumi Empirical	$ln(y_2') = a_0 + \frac{a_1}{T} + \frac{a_2}{T}\rho_1 - a_3 ln(P) + a_4 \ln(y_3\rho_1 T)$	5	(Soltani and Mazloumi, 2017)
	Soltani Mazloumi is an innovative experimental framework that incorporates five parameters to forecast solid solubility in supercritical carbon dioxide with the presence of a Co-solvent. This model considers various input data, including temperature, pressure, and density correlations. It is important to highlight that this model is derived from Hozhabr *et al.*'s model, showcasing a linear relationship between ln y_2' and ln P, a nonlinear association between ln y_2'' and temperature as well as density, a linear correlation between ln y_2' and a linear correlation between ln y_2'' and ln y_3 (Co-solvent mole fraction).		(Soltani Mazloumi, 2017)
Garlapati–Madras semi-empirical	$ln(y_2') = a_0 + a_1 ln(\rho_1) + a_2\rho_1 + \frac{a_3}{T} + a_4 ln(T) + a_5 ln(y_3) + a_6 ln(y_3\rho_1 T)$	7	(Saadati Ardestani et al., 2020)
	In 2010, the Garlapati–Madras equation was developed with seven constants, inspired by the model introduced by Jouyban et al. This equation is used to establish a relationship between the solubilities of high molecular weight solids in SC-CO_2, with or without Co-solvents, considering temperature, the density of SC-CO_2, and the mole fraction of Co-solvent.		(Garlapati and Madras, 2010)
Jouyban *et al.* Empirical	$\ln(y_2') = a_0 + a_1 y_3 + a_2\rho_1 + a_3 P^2 + a_4 PT + \frac{a_5 T}{P} + a_6 ln\rho_1$	7	(Jouyban et al., 2002b)
	The training of the proposed model to predict the solubilities of organic solids in SC-CO_2, considering the presence of a Co-solvent, utilizes a minimum of six experimental data points from the collected data sets. To estimate solubility at various temperatures and pressures, an interpolation technique was employed. This correlation provides numerous benefits, such as a simple calculation procedure and higher accuracy in comparison to other empirical equations and equations of state.		(Jouyban et al., 2002b)

Table 5
Descriptions of the parameters in empirical and semi-empirical models used in this work.

Parameter	Description	System
y_2	Mole fraction (RXN + SC-CO_2)	Binary system
y_2'	Mole fraction (RXN + SC-CO_2 + Ethanol)	Ternary system
y_3	The mole fraction of Co-solvent	Ternary system
$a_0 - a_5$	Adjustable parameters	Binary system
$a_0 - a_6$		Ternary system
ρ_1	Density of SC-CO_2 (kg m^{-3})	Binary & Ternary system
ρ_{ref}	Reference density (700 kg m^{-3})	Binary system
P_{ref}	Reference Pressure (0.1 MPa)	Binary & Ternary system
P	System Pressure (MPa)	Binary & Ternary system
T	System Temperature (K)	

the CO_2 tank, the liquid CO_2 enters the high-pressure pump at a pressure of about 6 MPa. A manometer and transmitter were used to evaluate the pressure with an accuracy of 0.1 MPa.

The drug was homogenized in SC-CO_2 using a magnetic stirrer in a 300-mL cell to achieve a lab balance cell (binary system). In the case of a ternary system or a Co-solvent approach, 3000 mg of the RXN was added to the cell with a certain amount (3 mol %) of ethanol as a Co-solvent. The temperature control was achieved using an oven. A sintered filter (1 μm) was placed to keep the RXN in place on either side of the cell. Before being fed to the cell, CO_2 was compressed to an appropriate pressure. Based on the preliminary test, the static time was 120 min. Saturated SC-CO_2 (600 μL ± 0.6 % μm) was inserted into the injection loop using a three-valve two-position device (shown by V_1-V_3) after 120 min. Upon rerouting the injection valve, the loop can be depressurized into the collecting vial to keep a particular amount of ethanol (solvent). This mechanism is summarized in Fig. 1 in four cases. After the static time, the loop should be filled. So, the valve (V_1) has been opened. After filling the loop, V_1 is closed. Next, V_2 is opened. The loop goes to the collection vial, then V_3 is opened and all the lines and the loop are rinsed with ethanol (1 mL). Also, in the picture, the green and black colors show the open and closed positions of the valves, respectively. This process was repeated three times for every data point and each system.

The solution was collected in a container with a final volume of 5 mL (±0.2 %). Each test was repeated multiple times. The absorbance was measured spectrophotometrically using a Jenway UV-V equipped with a quartz cell, at a maximum wavelength (λ_{max}) of 249 nm, to monitor the solubility. By utilizing the alignment bend (with a correlation coefficient of 0.989) and the UV absorbance, the solubility was calculated based on the solute concentration. The calibration curve and the linear relationship of the regression data over a wide concentration range confirmed the suitability of the method. Additionally, the melting point was estimated using the DSC test, as shown in Fig. 2. The calculation method for pressure fluctuation during sampling was also presented in the supplementary information, Table (S1).

The equilibrium mole fraction y_2 and solubility, S (g/L of RXN in SC-CO_2 were calculated at various pressure and temperature levels as follows (Sodeifian et al., 2023e):

$$y_2 = \frac{n_{solute}}{n_{solute} + n_{CO_2}} \tag{1}$$

$$n_{solute} = \frac{C_s\left(\frac{g}{L}\right) \times V_s(L)}{M_s\left(\frac{g}{mol}\right)} \tag{2}$$

$$n_{CO_2} = \frac{V_l(L) \times \rho\left(\frac{g}{L}\right)}{M_{CO_2}\left(\frac{g}{mol}\right)} \tag{3}$$

where C_s interprets the RXN concentration (g/L) in the collecting flask as determined by the standardized curve. n_{solute} and n_{CO2} also depict the moles of solute (RXN) and CO_2 in the sampling loop, respectively. The volumes of collecting vial and sampling loop were V_s (L) and V_l (L), respectively. The solute molecular weight is also shown by M_s (g/mol), while M_{CO2} stands for the molecular weight of carbon dioxide Eq. (4) was used to determine S (g/L), which is the concentration of RXN in the SC-CO_2.

Table 6
The experimental data of RXN solubility in SC-CO_2 based on distinct conditions.

Temperature[a] (K)	Pressure[a] (MPa)	Density[b] (kg/m^3)	Binary $y_2 \times 10^5$ (Mole Fraction)	Experimental standard deviation, S(y) × (10^5)[c]	$S \times 10$ (Solubility (g/l))	Expanded uncertainty of mole fraction (10^5), Uc[d]
308	12	768.42	0.405	0.007	0.031	0.011
	15	816.06	0.564	0.011	0.046	0.014
	18	848.87	0.745	0.018	0.063	0.020
	21	874.4	1.102	0.031	0.095	0.032
	24	895.54	1.248	0.041	0.111	0.043
	27	913.69	1.677	0.063	0.152	0.064
	30	929.68	1.924	0.080	0.177	0.081
318	12	659.73	0.256	0.006	0.017	0.011
	15	743.17	0.458	0.013	0.034	0.016
	18	790.18	0.676	0.022	0.053	0.023
	21	823.7	1.042	0.038	0.085	0.039
	24	850.1	1.389	0.059	0.117	0.060
	27	872.04	1.81	0.065	0.156	0.066
	30	890.92	2.163	0.087	0.191	0.088
328	12	506.85	0.171	0.003	0.009	0.012
	15	654.94	0.359	0.007	0.023	0.012
	18	724.13	0.593	0.014	0.043	0.017
	21	768.74	0.971	0.027	0.074	0.029
	24	801.92	1.57	0.054	0.125	0.056
	27	828.51	1.991	0.048	0.163	0.050
	30	850.83	2.396	0.069	0.202	0.071
338	12	384.17	0.102	0.003	0.004	0.016
	15	555.23	0.239	0.009	0.013	0.014
	18	651.18	0.48	0.019	0.031	0.021
	21	709.69	0.836	0.023	0.059	0.025
	24	751.17	1.71	0.055	0.127	0.056
	27	783.29	2.164	0.078	0.168	0.079
	30	809.58	2.572	0.007	0.206	0.019

[a] Standard uncertainty u are u(T) = 0.1 K; u(P) = 0.1 MPa.
[b] Data from the Span–Wagner equation of state.
[c] The experimental standard deviation and the experimental standard deviation of the mean (SD) were calculated by $S(y_k) = \sqrt{\frac{\sum_{j=1}^{n}(y_i - y)^2}{n-1}}$ and $SD(\overline{y}) = \frac{S(y_k)}{\sqrt{n}}$ respectively.
[d] The relative combined standard uncertainty was obtained by $U_{combined}/y = \sqrt{\sum_{i=1}^{N}(P_i U(x_i)/x_i)^2}$. The expanded uncertainty (0.95 level of confidence) U is $k \times U_{combined}$.

$$S\left(\frac{g}{L}\right) = \frac{C_s\left(\frac{g}{L}\right) \times V_s(L)}{V_l(L)} \tag{4}$$

As a result, Eq. (5) is produced by combining Eq. (2) and (3) with Eq. (1):

$$y_2 = \frac{C_s\left(\frac{g}{L}\right) \times V_s(L) \times M_{CO_2}\left(\frac{g}{mol}\right)}{C_s\left(\frac{g}{L}\right) \times V_s(L) \times M_{CO_2}\left(\frac{g}{mol}\right) + V_l(L) \times \rho\left(\frac{g}{L}\right) \times M_s\left(\frac{g}{mol}\right)} \tag{5}$$

2.3. Empirical and semi-empirical density-based models

Several empirical and semi empirical models can be used to determine the solubility of solids (drugs) in SC-CO_2. For the binary system in this study, the density-based models of Chrastil, Bian *et al.*, Jouyban *et al.*, Bartle *et al.*, Mendez – Santiago – Teja (MST), and Kumar-Johnston (KJ) were adopted. Concerning the ternary approach with ethanol (Co-solvent), the Garlapati–Madras, Sodeifian-Sajadian, MST, González *et al.*, Soltani-Mazloumi, and Jouyban *et al.* models were used. Empirical and semi-empirical models were employed to establish the connection between RXN solubility. Tables 4.a and 4.b provide a summary of the equations applied in binary and ternary approaches respectively and Table 5 outlines the parameters employed in the models.

Empirical and semi-empirical models' constants were assessed using experimental information. Variable parameters were also fine-tuned using the simulated annealing (SA) algorithm in MATLAB software. The AARD% was also applied to evaluate the accuracy of the model.

$$AARD\% = \frac{100}{N_i - Z}\sum_{i=1}^{N_i}\frac{\left|y_2^{calc} - y_2^{exp}\right|}{y_2^{exp}} \tag{6}$$

Z and N_i represent the number of modifiable parameters for any demonstration and the number of information focuses in any set or model, respectively (Sajadian et al., 2022b). R_{adj} was also considered to compare different models (Jouyban et al., 2002a, Garlapati and Madras, 2010):

$$R_{adj} = \sqrt{\left|R^2 - \left(\frac{Q(1-R^2)}{N-Q-1}\right)\right|} \tag{7}$$

Each set of data contained N data points. Moreover, Q denotes the number of self-determining

parameters of each equation. The R^2 correlation coefficient was also

Table 7
The experimental data of RXN solubility in SC-CO_2 – Ethanol based on distinct conditions. (3 mol % ethanol){, 2008 #1058}.

Temperature[a] (K)	Pressure[a] (MPa)	Density (kg/m^3)	Ternary $y_2' \times 10^4$ (Mole Fraction)	Experimental standard deviation, S (y $'$) $\times 10^{5b}$	Expanded uncertainty of mole fraction (1 0 ^{5}), Uc [c]	Mass ethanol (gr)	*e* (Co-solvent effect)
308	12	769.05	0.439	0.0755	0.080	7.463	10.84
	15	815.18	0.582	0.1164	0.122	7.926	10.32
	18	846.85	0.753	0.1807	0.187	8.244	10.11
	21	871.44	0.999	0.2797	0.286	8.492	9.07
	24	891.764	1.087	0.3594	0.365	8.698	8.71
	27	909.18	1.208	0.451	0.457	8.874	7.20
	30	924.51	1.34	0.5539	0.56	9.029	6.96
318	12	663.14	0.328	0.0787	0.082	6.407	12.81
	15	744.53	0.528	0.1542	0.158	7.218	11.53
	18	790.14	0.763	0.2442	0.249	7.674	11.29
	21	822.57	1.031	0.3712	0.377	8.000	9.89
	24	848.04	1.208	0.5154	0.251	8.256	8.70
	27	869.17	1.441	0.5188	0.527	8.469	7.96
	30	887.32	1.603	0.6412	0.649	8.653	7.41
328	12	512.60	0.26	0.0458	0.050	4.923	15.20
	15	658.45	0.442	0.0884	0.093	6.361	12.31
	18	726.00	0.708	0.1699	0.176	7.033	11.94
	21	769.36	1.004	0.2811	0.288	7.466	10.34
	24	801.51	1.45	0.5027	0.510	7.788	9.24
	27	827.21	1.566	0.3758	0.388	8.047	7.87
	30	848.74	1.794	0.5191	0.531	8.263	7.49
338	12	390.45	0.191	0.0611	0.065	3.731	18.73
	15	560.44	0.387	0.1393	0.142	5.393	16.19
	18	654.77	0.652	0.2608	0.264	6.324	13.58
	21	711.93	1.079	0.3021	0.310	6.893	12.91
	24	752.30	1.635	0.5232	0.533	7.296	9.56
	27	783.47	1.846	0.6646	0.674	7.607	8.53
	30	808.92	2.022	0.8088	0.819	7.863	7.86

[b] The experimental standard deviation and the experimental standard deviation of the mean (SD) were calculated by $S(y_k) = \sqrt{\frac{\sum_{j=1}^{n}(y_i - y)^2}{n-1}}$ and $SD(\bar{y}) = \frac{S(y_k)}{\sqrt{n}}$ respectively.

[a] Standard uncertainty u are u(T) = 0.1 K; u(P) = 0.1 MPa.

[c] The relative combined standard uncertainty was obtained by $U_{combined}/y = \sqrt{\sum_{i=1}^{N}(P_i U(x_i)/x_i)^2}$. The expanded uncertainty (0.95 level of confidence) U is $k \times U_{combined}$.

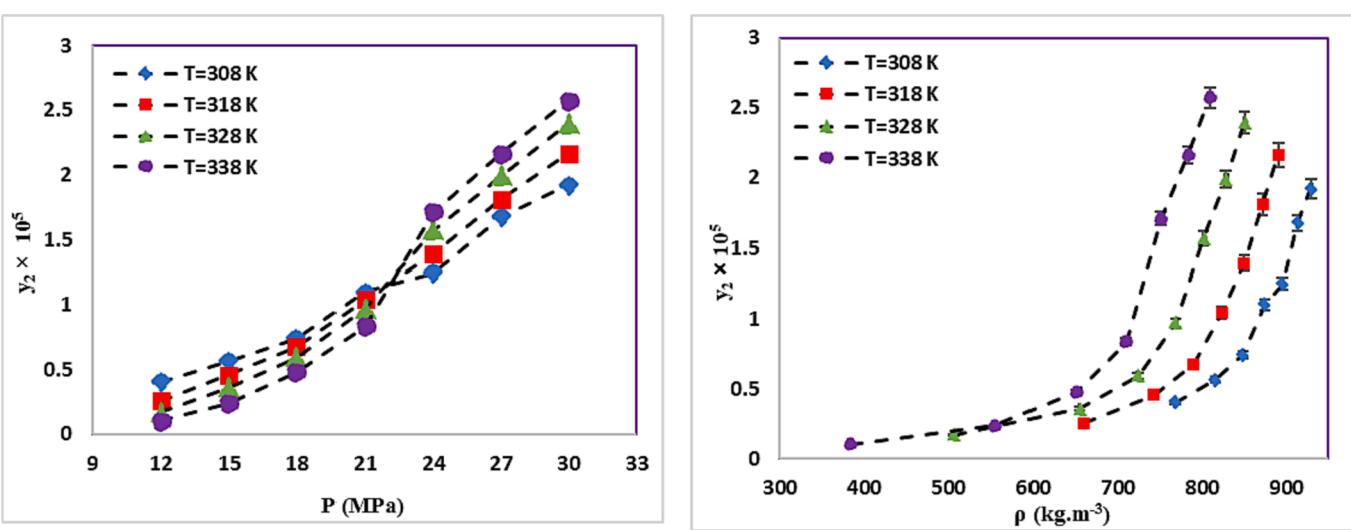

Fig. 3. The RXN solubility in the binary system.

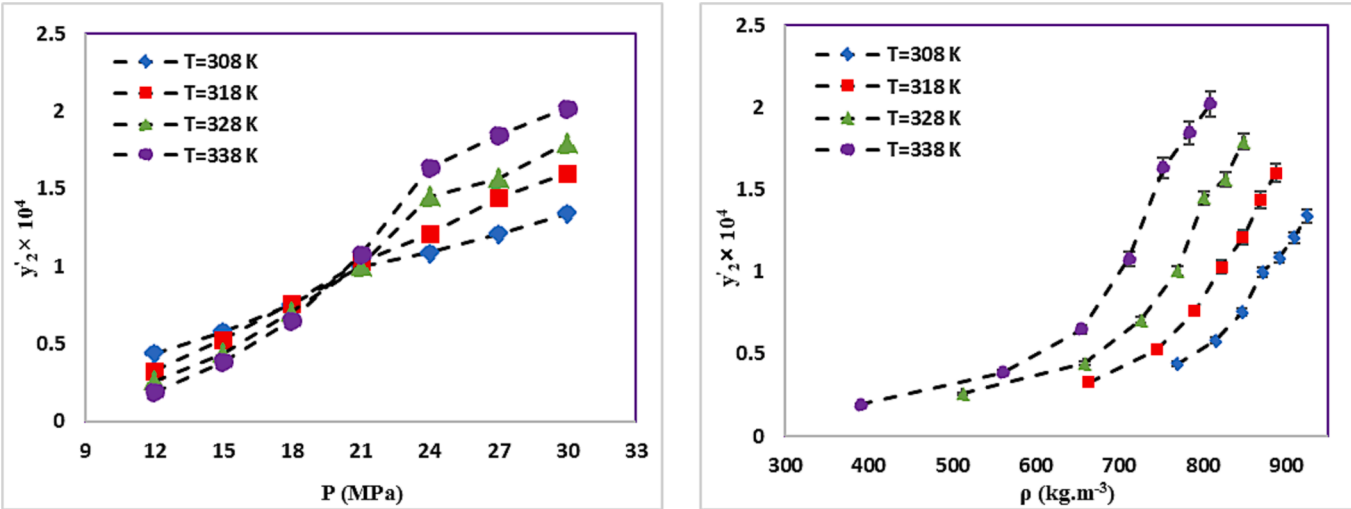

Fig. 4. The RXN solubility in the ternary system.

used to compare different models:

$$R^2 = 1 - \frac{SS_E}{SS_T} = 1 - \frac{\sum (y_{2\exp} - y_2)^2}{\sum (y_{2\exp})^2 - \frac{(\Sigma y)^2}{N}} \quad (8)$$

Where SS_E represents the sum square error and SS_T denotes the total sum of squares (Sodeifian et al., 2019e).

3. Results and discussion

3.1. Solubility data systems- role of Co-solvent

The experimental solubilities of RXN in SC-CO_2 with and without ethanol Co-solvent (ternary and binary) were explored experimentally at 308–338 K and 12–30 MPa, as reported in Tables 6 and 7. The Span-Wanger EoS was used to determine the SC-CO_2 density (Span and Wagner, 1996). Additionally, each test was reassessed three times to enhance the precision, and the relative standard uncertainties fell below 5 %. The uncertainty of solubility was determined according to the guide of uncertainty measurement (GUM) proposed by the joint committee for guides in metrology (2008). Figs. 3 and 4 present the RXN mole fraction solubility vs. pressure and density at various temperatures for binary and ternary systems, respectively. In 2022, Sodeifian *et al.* studied RXN in binary mode. According to Table 6, the data difference is lower than 9 % (Sodeifian et al., 2023e). The supplementary information data consists of Tables S2 and S3, containing the tabulated information necessary for the calculation and analysis of ethanol (Co-solvent) content, mixture density, and CO_2 mass within the mixture.

In general, an increase in pressure enhances the density of SC-CO_2 and its solvation power. Consequently, the solubility of RXN in SC-CO_2 increases with pressure increment at constant temperature in both systems. Analysis of RXN solubility in binary and ternary systems indicates a significant increase in the solubility of RXN in the presence of a Co-solvent (ethanol). According to the generally recognized as safe (GRAS) designation, ethanol is an ideal Co-solvent for food applications (Güçlü-Üstündağ and Temelli, 2005). The maximum and minimum effects of the Co-solvent are 18.73 (338 K and 12 MPa) and 6.96 (308 K and 30 MPa), respectively, as determined by comparing the data and calculating the solubility enhancement (e) due to the efficacy of ethanol Co-solvent on the RXN solubility in SC-CO_2 (Eq. (9) (Araus et al., 2019, Sodeifian et al., 2021).

$$e = \frac{y_2'}{y_2} * 100 = \frac{molefractionofTernary(CO_2 + Ethanol)}{molefractionofbinary(CO_2)} * 100 \quad (9)$$

In addition, as illustrated in Fig. 5, the impact of ethanol on solubility is identified. The addition of a Co-solvent results in a solubility increase ranging from 7 to 19 % in the ternary system when compared to the binary system.

CO_2 cannot be employed as a suitable solvent for most medicinal chemicals due to its low polarity. Moreover, hydrophobic and polar molecules are insoluble in SC-CO_2. Therefore,

variant Co-solvents have been introduced to enhance the solubility of drugs in SC-CO_2. Ethanol is miscible with SC-CO_2 and has shown a high dissolving capacity for numerous chemicals. Thus, ethanol can be employed as a Co-solvent in SC-CO_2 systems to improve the dissolving capability (Knez et al., 2017, Cheng et al., 2018).

Small concentrations of Co-solvents can be used to increase the solvation power of SC-CO_2. The effect of the Co-solvent was determined based on its concentration in the supercritical phase, which can be influenced by the phase and the treatment of the combination. To determine the influence of the Co-solvent, solvent-co-solvent combinations in a supercritical state (completely miscible) should be used (Güçlü-Üstündağ and Temelli, 2005, Pitchaiah et al., 2018). The key factor in the effect of the Co-solvent involves an increase in solvent density and intermolecular interactions. In multi-component systems, solubility can be improved either selectively or non-selectively. Selectivity does not increase in situations where the rise in insolubility is the result of an increment in the density of the solvent mixture. An increase is expected in both solubility and selectivity in the case of a specific intermolecular interaction between the Co-solvent and one of the solutes (such as H-bonding) (Güçlü-Üstündağ and Temelli, 2005, Cui et al., 2018, Li et al., 2018).

The impact of Co-solvent on solvent density, and therefore its contribution to the Co-solvent effect, varies depending on temperature and the specific Co-solvent. The inclusion of a Co-solvent increases the overall density of the supercritical fluid (SCF) by raising the density of the Co-solvent and causing SCF molecules to cluster around it. These density variations are particularly noticeable near the critical point of the solvent mixture, where the densities of both the Co-solvent and the

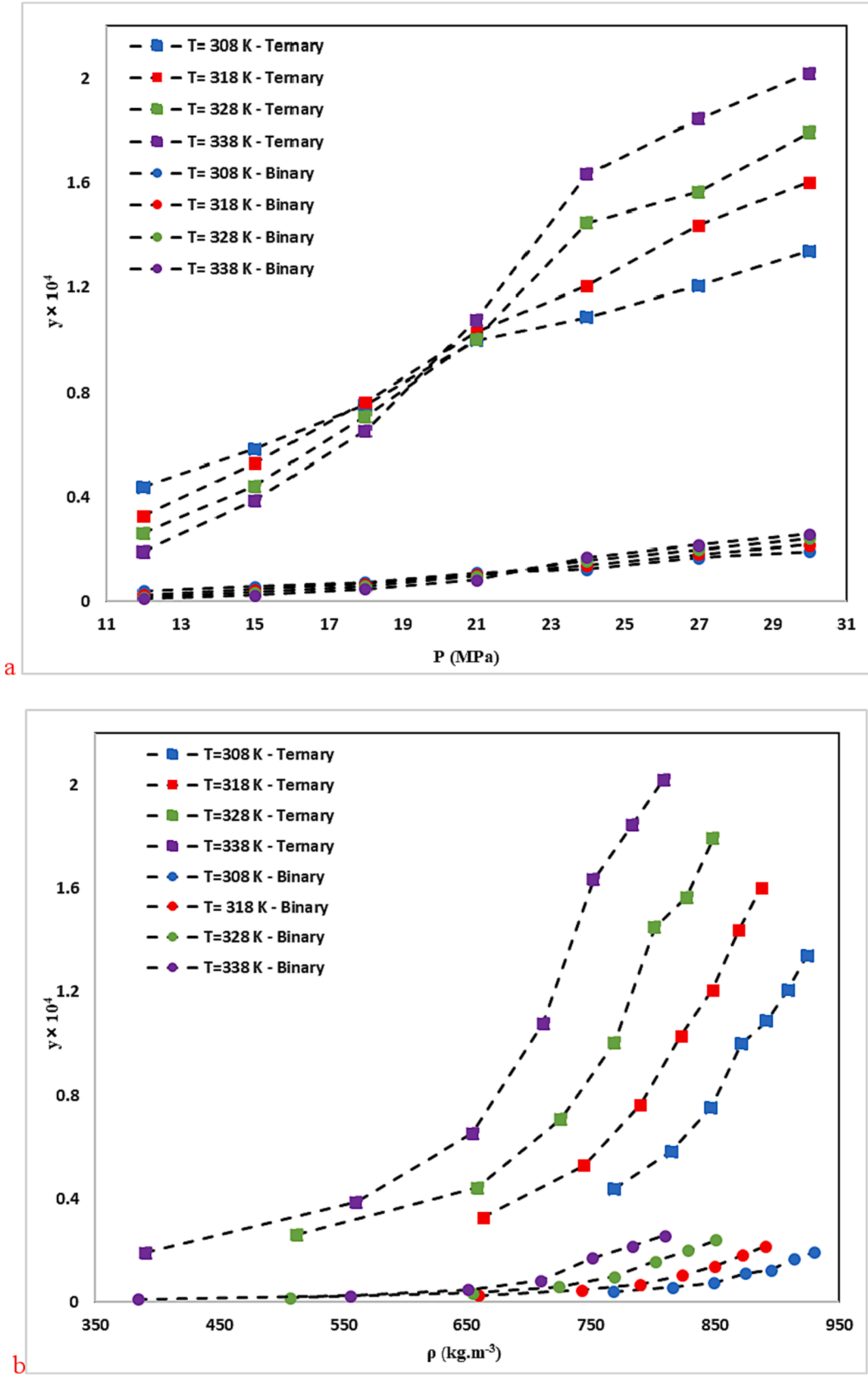

Fig. 5. The influence of Co-solvent (ethanol) on solubility of RXN in SC-CO_2. a. pressure, b. density.

Table 8
The correlation results of the RXN-CO_2 system provided by semi-empirical models.

Model	a_0	a_1	a_2	a_3	a_4	a_5	*AARD%*	R_{adj}
Chrastil	8.794	−5323.289	−43.942	–	–	–	16.75	0.989
KJ	−2.449	0.009	−5352.72	–	–	–	12.42	0.989
Bian et al.	−4.736	0.003	−2324.664	−3.713	17.185	–	8.05	0.986
Bartle *et al.*	16.928	−7878.695	0.014	–	–	–	16.79	0.986
MST	4.797	-1.182×10^{-4}	18.672	–	–	–	15.93	0.990
Jouyban *et al.*	–33.695	0.002	−0.004	9.689×10^{-5}	0.100	2.062	7.40	0.993

Table 9
The correlation results of the RXN-Ethanol-CO_2 system provided by the semi-empirical models.

Model	a_0	a_1	a_2	a_3	a_4	a_5	a_6	*AARD%*	R_{adj}
MST	−1920.282	3.510	16.855	-2.517×10^{-5}	–	–	–	12.37	0.986
González *et al.*	5.450	−2.867	-4.498×10^{4}	−41.694	–	–	–	12.17	0.985
Sodeifian-Sajadian	−2.360	−0.482	0.018	0.695	–	–	–	6.13	0.979
Soltani-Mazloumi	4.608	−5194.273	1.885	−0.386	−0.495	–	–	6.89	0.987
Garlapati–Madras	−93.651	−6.345	0.011	−26.658	10.571	−8.462	3.027	6.16	0.991
Jouyban *et al.*	−50.732	−1.899	−0.007	−0.002	5.083×10^{-4}	0.008	6.70	9.39	0.989

SCF fluctuate the most, resulting in the highest degree of clustering. As the pressure increases, the density of the SCF mixture increases while the clustering decreases, causing the density isotherms to intersect. It should be noted that the addition of a Co-solvent, such as a hydrocarbon with a large molar volume, can enhance the solvation power of the SCF while reducing its molar density (Güçlü-Üstündağ and Temelli, 2005, Li et al., 2018).

A proper understanding of the Co-solvent outcome demands sufficient cognition of the intermolecular interactions between the solutes and solvents. The Co-solvent effect is mostly influenced by solute-co-solvent physical interactions such as dipole–dipole, dipole-induced dipole, and induced dipole-induced dipole (dispersion) interactions, as well as more specialized interactions such as H-bonding and charge transfer complexes (Prausnitz et al., 1999, Güçlü-Üstündağ and Temelli, 2005, Cui et al., 2018, Peyrovedin and Shariati, 2020, Matin et al., 2022).

H-bonding could be a donor–acceptor action and reaction, including H-bond- donating and accepting atoms. H-bonds are formed when the electronegativity of the H-bond donor is sufficiently high to draw electrons, partially exposing the protons. The acceptor atom has to possess lone-pairs or polarizable electrons to form a bond with the donor species. Functional groups could serve as acceptors (e.g., C = O), donors, or both (e.g., OH). As the most prevalent cases in essence and chemistry, moderate H-bonds are generated between neutral donors and acceptors like –OH and O = C (Jeffrey and Jeffrey, 1997). In the mixture of SC-CO_2 and ethanol, ethanol forms H-bonds for weak binding to CO_2 as a result of quadrupole-dipole interaction. Furthermore, the hydrogen bonding between RXN and this Co-solvent declined chemical potential, offering additional solute molecules to the supercritical phase (Güçlü-Üstündağ and Temelli, 2005, Araus et al., 2019, Ardestani et al., 2020).

Several articles have investigated crossover pressure and proposed some methods to predict the crossover pressure region (Adachi and Lu, 1983, Chimowitz et al., 1988, Del Valle and Aguilera, 1988, de Melo et al., 2009, Tabernero et al., 2010, Budkov et al., 2019, Kalikin et al., 2020, Kalikin et al., 2021). Correlation of the crossover pressure for the ternary system has been presented by Johnston *et al.*(Adachi and Lu, 1983) and Chimowitz *et al.*(Chimowitz et al., 1988). The crossover pressure was related to the enthalpy of sublimation and the partial molar enthalpy of the solute in the supercritical phase. The locations of the lower and upper crossover pressures were determined at the point where the partial molar enthalpy equals the negative of the enthalpy of sublimation. Johnston *et al.* (1987) applied the Peng-Robinson EoS with a binary interaction parameter regressed from a single experimental point to evaluate the partial molar enthalpy of the solute for determining the crossover points. Chimowitz et al. (1988) used a perturbed hard-sphere model EoS to correlate the crossover pressure for binary and ternary systems. Both of these methods require the P-y-T data to allow the prediction of the crossover point. Kalikin *et al.* (Kalikin et al., 2021) investigated the solubility of a set of poorly soluble drugs, which have been computed in a wide area of the phase diagram, based on the classical density functional theory. They found that the wider the temperature region of the experimental study, the more pronounced the effect of the crossover points drift. They also estimated solubility values using in situ IR spectroscopy and molecular dynamics simulations along the mentioned isochores and isotherms, respectively. Furthermore, they believed that the critical parameters, sublimation pressure, and molar volume of the compound play a crucial role in the determination of the crossover pressure (Tabernero et al., 2010). De Melo *et al.* investigated the Peng-Robinson-LCVM-UNIFAC equation and the effect of any uncertainty of some solid pure component properties on the upper crossover pressure. It is shown that the slope of the sublimation pressure curve plays a major role in the accuracy of the upper crossover pressure. To sum up, the crossover region depends on the critical properties of solutes, sublimation pressure, enthalpy of sublimation, partial molar enthalpy, and molar volume of the solute.

As suggested by the chemical structure of RXN (Table 3), its OH, NH, and C = O groups increase its polarity. Accordingly, the solubility of RXN in a high-density solvent will be higher than in a low-density solvent for both binary and ternary systems. At high pressures, SCF behaves like a liquid. Regarding the higher solvation power of liquids compared to gases, RXN is more soluble in solvents with higher density (see Fig. 4). Temperature is another key factor in the solubility of RXN. Based on Figs. 3 and 4, the solubility of RXN in both binary and ternary systems increased with constant pressure, due to temperature elevation. The binary and ternary systems showed crossover pressures. Concerning the solubility of solid materials in supercritical fluids, there is a well-known phenomenon called “retrograde vaporization” (RV), in which a rise in temperature at steady pressure causes a decline in solubility (Kalikin

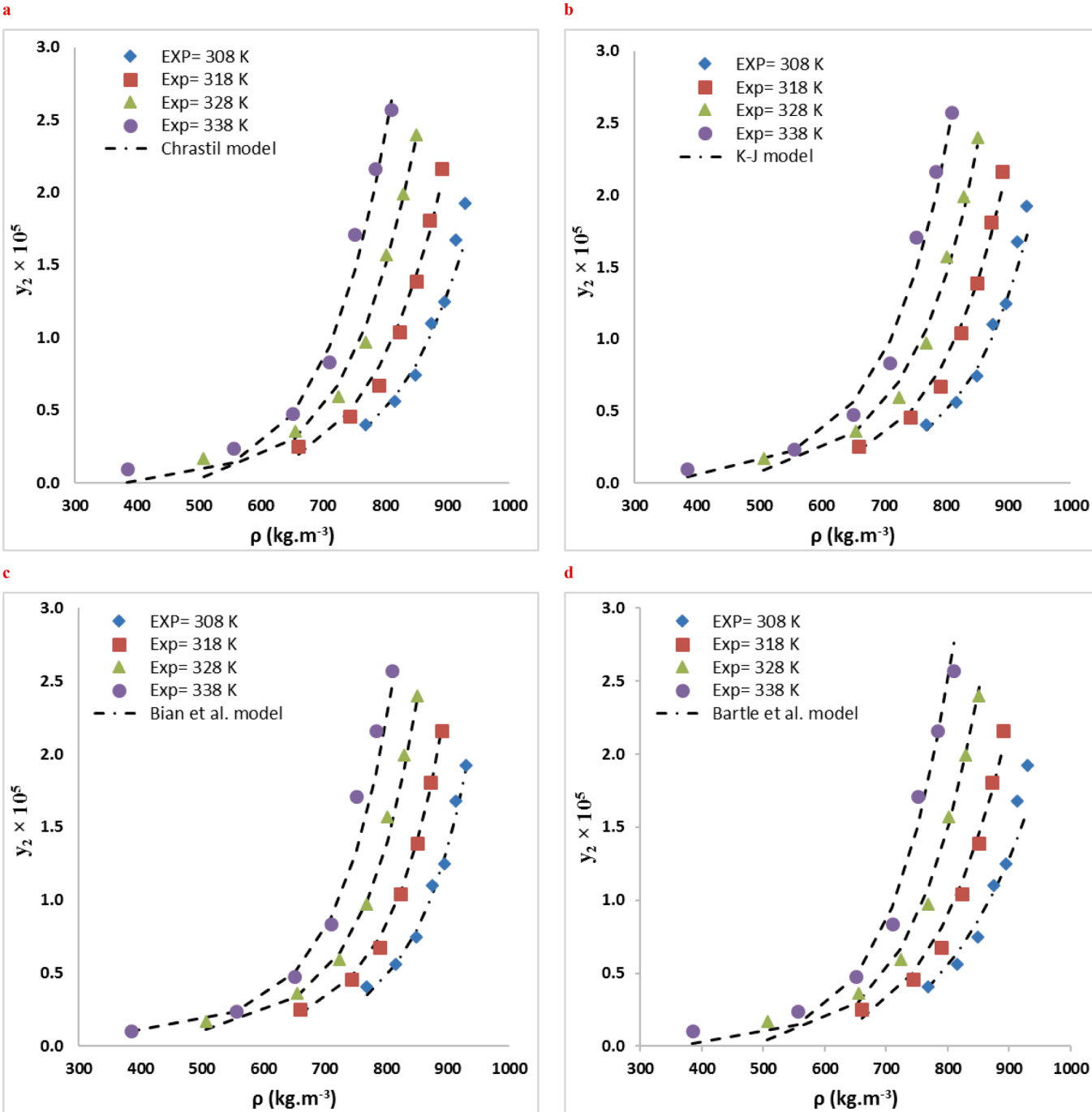

Fig. 6. Comparison of experimental (points) and calculated (line) solubilities of RXN in the binary system: (a) Chrastil, (b) KJ., (c) Bian *et al* (d) Bartle *et al*, (e) MST (f) Jouyban *et al.* models at various temperatures.

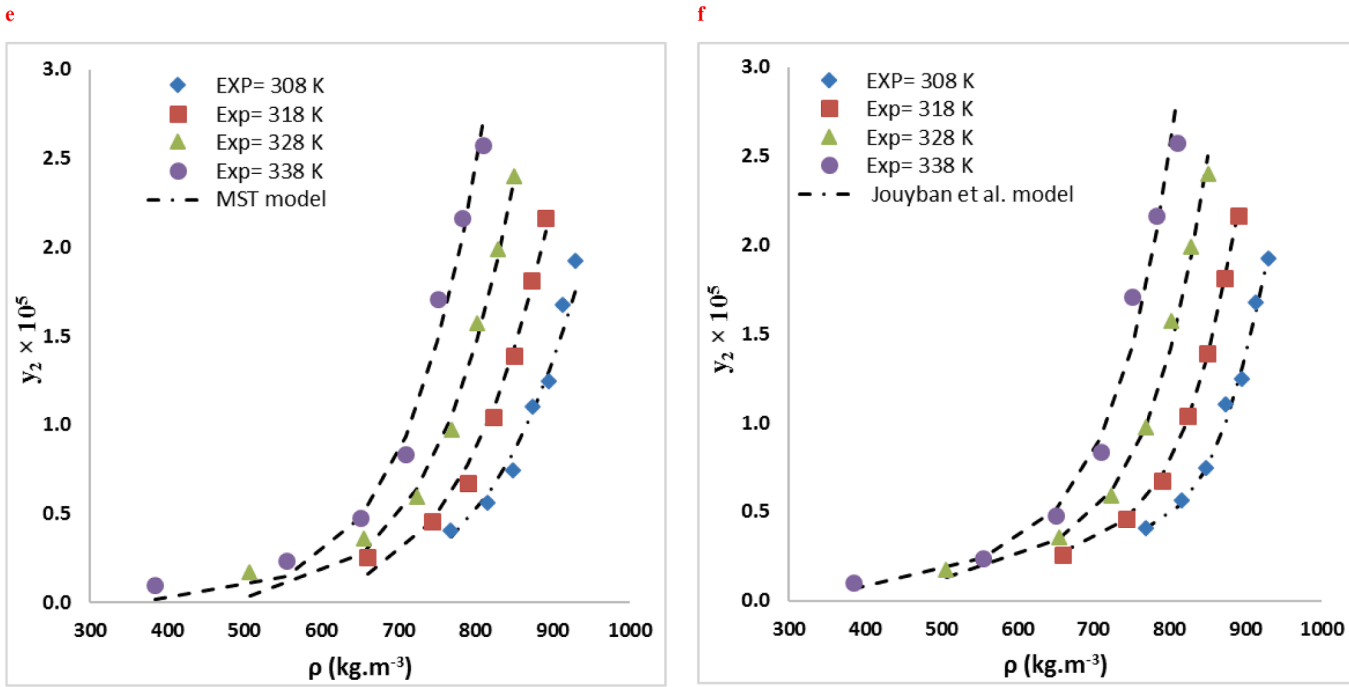

Fig. 6. (*continued*).

et al., 2021). The limits of this area are illustrated by two positions where all isotherms intersect and the plot of solubility vs. temperature shows extrema; the pressure values corresponding to these extrema are known as the lower and upper crossover pressures. In the case of binary and ternary systems, the crossover pressures roughly reside at 24 MPa and 21 MPa, respectively. The temperature of the system shows different impacts on RXN solubility at pressures higher and lower than the crossover pressure. The effects of temperature enhancement on solubility may vary due to the temperature dependence of the density of the solvent and the vapor pressure of the solute.

3.2. Analyzed solubility data correlation of two system

RXN solubility data were compared in two systems using ten empirical density-based models (Bian *et al.*, Jouyban *et al.*, Chrastil, Bartle *et al.*, Mendez – Santiago – Teja (MST), González *et al.*, Kumar, and Johnston (KJ), Sodeifian–Sajadian, Soltani-Mazloumi and Garlapati-Madras). The RXN solubility in SCF was correctly correlated by all correlations, as shown by the AARD% and Radj values. Using the calculated customizable parameters, the offered models may be employed to predict RXN solubility in binary and ternary modes at definite pressures and temperatures. The solubility data were correlated with high precision using the acquired adjustable parameters. Tables 8 and 9 list the parameters of the empirical and semi empirical model in the binary RXN-CO_2 system and the ternary RXN-Ethanol-CO_2 system, respectively. The correlation outcomes of each approach are displayed in Figs. 6 and 7. The AARD% of each model in both systems is shown in Fig. 8. Additionally, Jouyban *et al.* (AARD%=7.40 and R_{adj} = 0.993) is the most accurate model in the binary system. As seen, all models provide proper accuracy in ternary models, while the Garlapati-Madras (AARD%=6.16 and R_{adj} = 0.991) and Sodeifian-Sajadian (AARD%= 6.13 and R_{adj} = 0.979) and Soltani-Mazloumi (AARD%=6.89 and R_{adj} = 0.987) models for the ternary system are the most accurate models.

4. Conclusion

The current research explored the RXN solubility in two systems (binary: SC-CO_2 and ternary: SC-CO_2 with Co-solvent (ethanol) at different pressures (12–30 MPa) temperatures (308–338 K). The RXN solubility in the binary and ternary systems ranged based on mole fraction from 1.0×10^{-6} to 2.57×10^{-5} and from 1.9×10^{-5} to 2.02×10^{-4}, respectively. The solubility values of RXN were correlated by various semi-empirical equations based on the corresponding equilibrium. Accordingly, the incorporation of ethanol Co-solvent considerably improved the RXN solubility due to dipole–dipole and dipole-induced dipole interactions between the Co-solvent and RXN. The highest Co-solvent effect (18.73) was identified at 12 MPa and 338 K, further confirming this hypothesis. The highest RXN solubility ($y'_2 = 2.02 \times 10^{-4}$) at 30 MPa and 338 K, was recorded in a system with ethanol Co-solvent. Furthermore, according to the AARD% and R_{adj} values of the empirical and semi-empirical approaches, Jouyban *et al.* model for binary system and Garlapati-Madras, Sodeifian-Sajadian and Soltani-Mazloumi models can properly correlate the ternary system at examined temperatures and pressures.

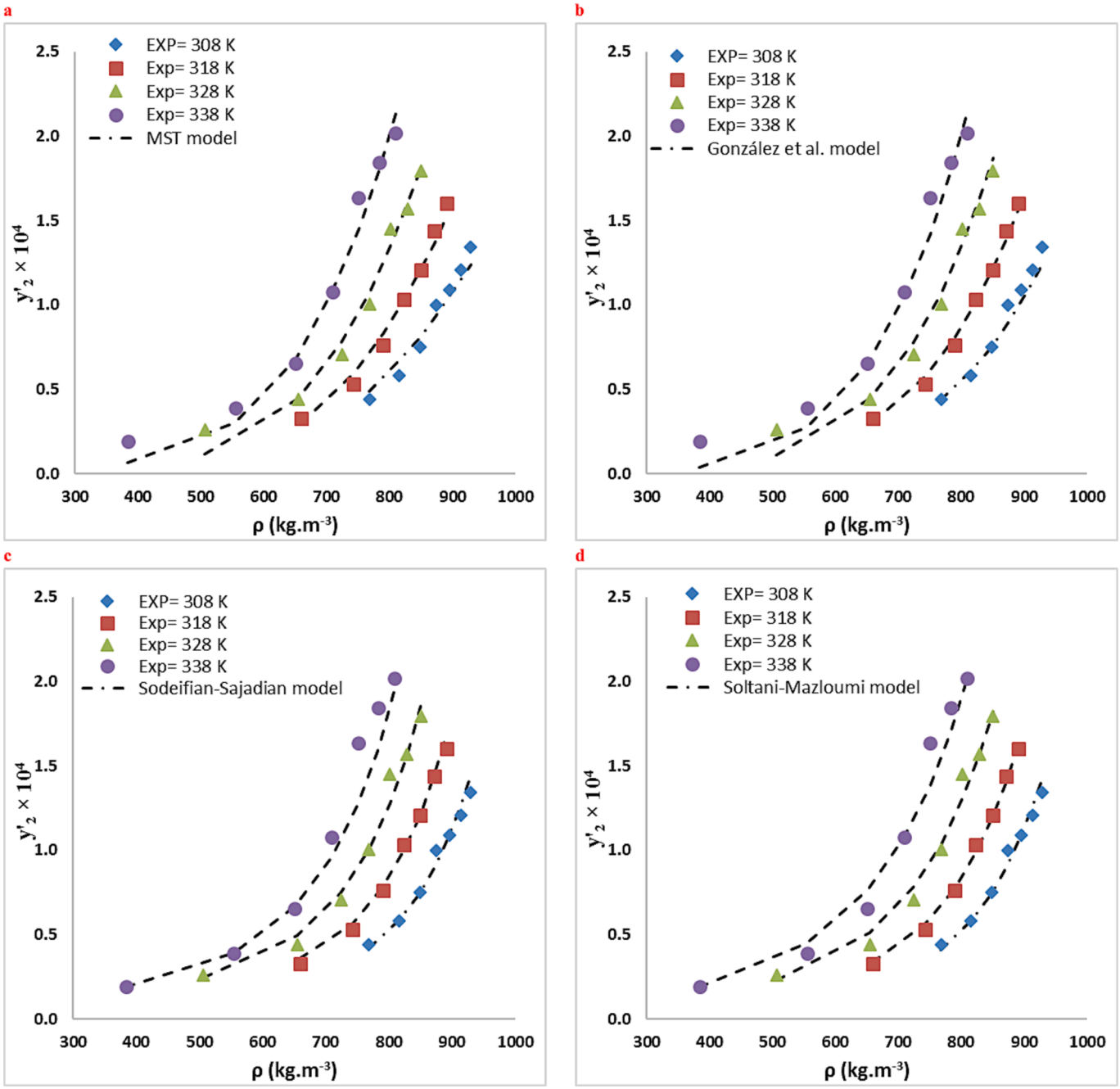

Fig. 7. Comparison of experimental (points) and calculated (line) solubilities of RXN in the ternary system (3 mol % ethanol): (a) MST, (b) González *et al.*, (c) Sodeifian-Sajadian, (d) Soltani-Mazloumi. (e) Garlapati–Madras and (f) Jouyban *et al.* models at various temperatures.

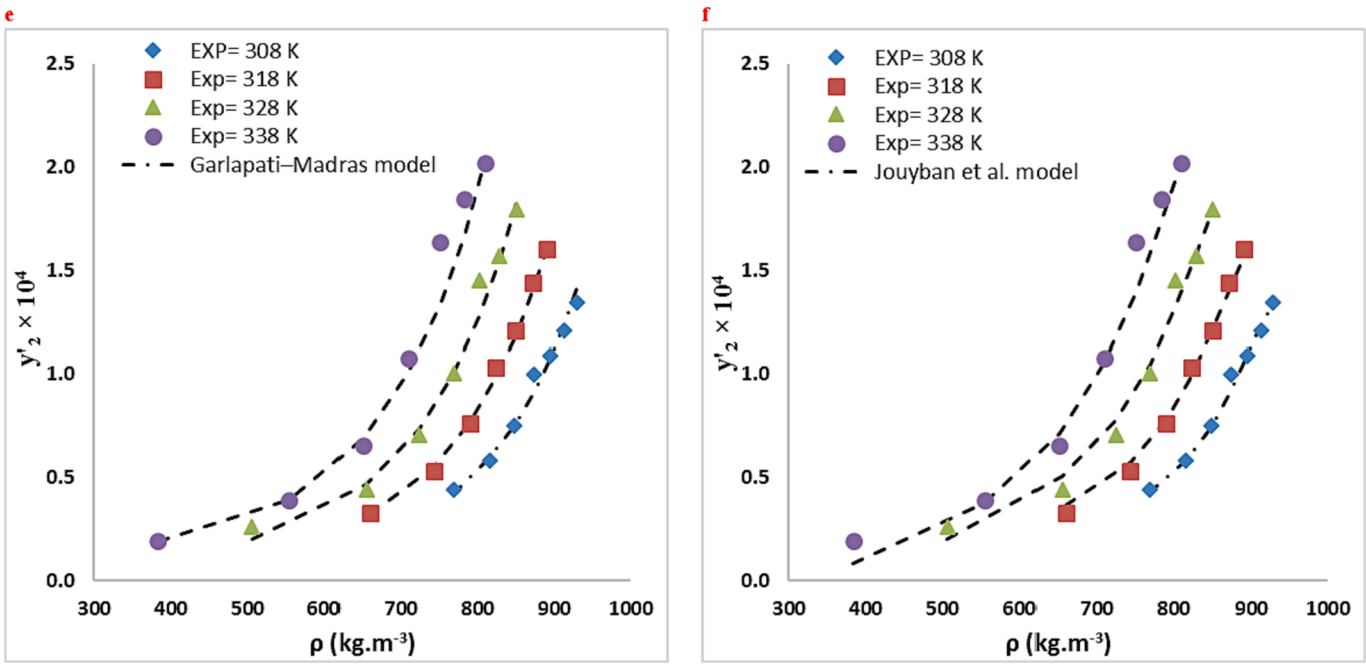

Fig. 7. (*continued*).

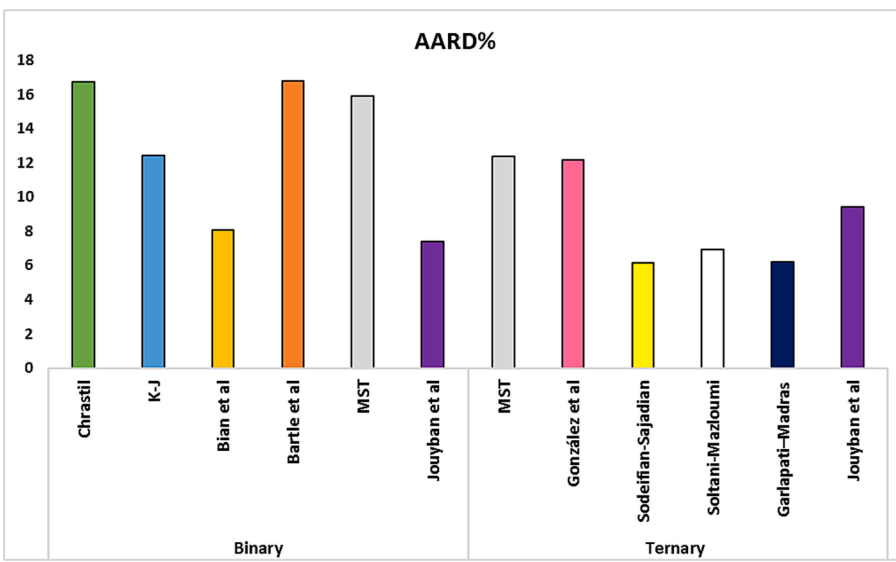

Fig. 8. Comparing ARRD percentages between Binary and Ternary models.

CRediT authorship contribution statement

M.A.: Methodology, Writing- Original draft preparation, Data curation and Software, Reviewing and Editing. N.E.: Methodology, Writing-Original draft preparation, Conceptualization, Investigation, Validation, funding acquisition, Reviewing and Editing. B.H.: Validation, Methodology, Investigation, Reviewing. S.A.S.: Conceptualization, Project administration, Software, Supervision, Reviewing and Editing. A.A.: Investigation, Writing, Reviewing and Editing.

Declaration of Competing Interest

The authors declare that they have no known competing financial interests or personal relationships that could have appeared to influence the work reported in this paper.

Appendix A. Supplementary data

Supplementary data to this article can be found online at https://doi.org/10.1016/j.arabjc.2024.105707.

References

Abadian, M., Sodeifian, G., Razmimanesh, F., et al., 2022. Experimental measurement and thermodynamic modeling of solubility of Riluzole drug (neuroprotective agent) in supercritical carbon dioxide. Fluid Phase Equilibria. 113711 https://doi.org/10.1016/j.fluid.2022.113711.

Abourehab, M.A.S., Alshehri, S., Alzhrani, R.M., et al., 2022b. Experimental evaluation and thermodynamic analysis of Febuxostat solubility in supercritical solvent. Journal of Molecular Liquids. 364, 120040. https://doi.org/10.1016/j.molliq.2022.120040.

Abourehab, M.A., Alsubaiyel, A.M., Alshehri, S., et al., 2022a. Laboratory determination and thermodynamic analysis of alendronate solubility in supercritical carbon dioxide. Journal of Molecular Liquids. 367, 120242. https://doi.org/10.1016/j.molliq.2022.120242.

Adachi, Y., Lu, B.-C.-Y., 1983. Supercritical fluid extraction with carbon dioxide and ethylene. Fluid Phase Equilibria. 14, 147–156. https://doi.org/10.1016/0378-3812(83)80120-4.

Alharby, T.N., Algahtani, M.M., Alanazi, J., et al., 2023. Advancing nanomedicine production via green thermal supercritical processing: Laboratory measurement and thermodynamic modeling. Journal of Molecular Liquids. 383, 122042. https://doi.org/10.1016/j.molliq.2023.122042.

Alshahrani, S.M., Alsubaiyel, A.M., Abduljabbar, M.H., et al., 2023. Measurement of metoprolol solubility in supercritical carbon dioxide; experimental and modeling study. Case Studies in Thermal Engineering. 42, 102764. https://doi.org/10.1016/j.csite.2023.102764.

Alshehri, S., Alqarni, M., Namazi, N.I., et al., 2022. Design of predictive model to optimize the solubility of Oxaprozin as nonsteroidal anti-inflammatory drug. Scientific Reports. 12, 13106. https://doi.org/10.1038/s41598-022-17350-5.

Alwi, R.S., Rojas, A., Esfandiari, N., et al., 2023. Experimental study and thermodynamic modeling of clonazepam solubility in supercritical carbon dioxide. Fluid Phase Equilibria. 113880 https://doi.org/10.1016/j.fluid.2023.113880.

Amani, M., Ardestani, N.S., Jouyban, A., et al., 2022. Solubility measurement of the fludrocortisone acetate in supercritical carbon dioxide: Experimental and modeling assessments. The Journal of Supercritical Fluids. 190, 105752. https://doi.org/10.1016/j.supflu.2022.105752.

Ansari, E., Honarvar, B., Sajadian, S.A., et al., 2023. Solubility of Aripiprazole in Supercritical Carbon Dioxide: Experimental and Modeling Evaluations. https://doi.org/10.1038/s41598-023-40537-3.

Araus, K.A., Casado, V., del Valle, J.M., et al., 2019. Cosolvent effect of ethanol on the solubility of lutein in supercritical carbon dioxide. The Journal of Supercritical Fluids. 143, 205–210. https://doi.org/10.1016/j.supflu.2018.08.012.

Ardestani, N.S., Majd, N.Y., Amani, M., 2020. Experimental Measurement and Thermodynamic Modeling of Capecitabine (an Anticancer Drug) Solubility in Supercritical Carbon Dioxide in a Ternary System: Effect of Different Cosolvents. Journal of Chemical & Engineering Data. 65, 4762–4779. https://doi.org/10.1021/acs.jced.0c00183.

Ardestani, N.S., Sajadian, S.A., Esfandiari, N., et al., 2023. Experimental and modeling of solubility of sitagliptin phosphate, in supercritical carbon dioxide: proposing a new association model. Scientific Reports. 13, 17506. https://doi.org/10.1038/s41598-023-44787-z.

Askarizadeh, M., Esfandiari, N., Honarvar, B., et al., 2023. Kinetic modeling to explain the release of medicine from drug delivery systems. ChemBioEng Reviews. 10, 1006–1049. https://doi.org/10.1002/cben.202300027.

Bagheri, H., Notej, B., Shahsavari, S., et al., 2022. Supercritical carbon dioxide utilization in drug delivery: Experimental study and modeling of paracetamol solubility. European Journal of Pharmaceutical Sciences. 177, 106273. https://doi.org/10.1016/j.ejps.2022.106273.

Bartle, K., Clifford, A., Jafar, S., et al., 1991. Solubilities of solids and liquids of low volatility in supercritical carbon dioxide. Journal of Physical and Chemical Reference Data. 20, 713–756. https://doi.org/10.1063/1.555893.

Bazaei, M., Honarvar, B., Esfandiari, N., et al., 2023. Measurement and thermodynamic modeling of solubility of Erlotinib hydrochloride, as an anti-cancer drug, in supercritical carbon dioxide. Fluid Phase Equilibria. 113877 https://doi.org/10.1016/j.fluid.2023.113877.

Bian, X., Du, Z., Tang, Y., 2011. An improved density-based model for the solubility of some compounds in supercritical carbon dioxide. Thermochimica Acta. 519, 16–21. https://doi.org/10.1016/j.tca.2011.02.023.

Bitencourt, R.G., Palma, A.M., Coutinho, J.A., et al., 2019. Prediction of solid solute solubility in supercritical CO2 with cosolvents using the CPA EoS. Fluid Phase Equilibria. 482, 1–10. https://doi.org/10.1016/j.fluid.2018.10.020.

Budkov, Y., Kolesnikov, A., Ivlev, D., et al., 2019. Possibility of pressure crossover prediction by classical dft for sparingly dissolved compounds in scco2. Journal of Molecular Liquids. 276, 801–805. https://doi.org/10.1016/j.molliq.2018.12.021.

Capell, W.H., Barnathan, E.S., Piazza, G., et al., 2021. Rationale and design for the study of rivaroxaban to reduce thrombotic events, hospitalization and death in outpatients with COVID-19: The PREVENT-HD study. American Heart Journal. 235, 12–23. https://doi.org/10.1016/j.ahj.2021.02.001.

Chen, C.-T., Lee, C.-A., Tang, M., et al., 2017. Experimental investigation for the solubility and micronization of pyridin-4-amine in supercritical carbon dioxide. Journal of CO2 Utilization. 18, 173–180. https://doi.org/10.1016/j.jcou.2017.01.020.

Cheng, J., Han, S., Song, J., et al., 2018. Solubility of vitamin E acetate in supercritical carbon dioxide with ethanol as cosolvent. Journal of Chemical & Engineering Data. 63, 4248–4255. https://doi.org/10.1021/acs.jced.8b00745.

Chimowitz, E., Kelley, F., Munoz, F., 1988. Analysis of retrograde behavior and the cross-over effect in supercritical fluids. Fluid Phase Equilibria. 44, 23–52. https://doi.org/10.1016/0378-3812(88)80102-x.

Chrastil, J., 1982. Solubility of solids and liquids in supercritical gases. The Journal of Physical Chemistry. 86, 3016–3021. https://doi.org/10.1021/j100212a041.

Ciou, J.-M., Wang, B.-C., Su, C.-S., et al., 2018. Measurement of solid solubility of warfarin in supercritical carbon dioxide and recrystallization study using supercritical antisolvent process. Advanced Powder Technology. 29, 479–487. https://doi.org/10.1016/j.apt.2017.12.005.

Costa, O.S., Thompson, S., Ashton, V., et al., 2020. Rivaroxaban versus warfarin for treatment and prevention of recurrence of venous thromboembolism in African American patients: a retrospective cohort analysis. Thrombosis Journal. 18, 1–9. https://doi.org/10.1186/s12959-020-00219-w.

Cui, C.-L., Shi, W., Long, J.-J., 2018. Solubility and data correlation of a reactive disperse dye in a quaternary system of supercritical carbon dioxide with mixed cosolvents. Journal of the Taiwan Institute of Chemical Engineers. 91, 213–223. https://doi.org/10.1016/j.jtice.2018.06.028.

de Melo, S.V., Costa, G.M.N., Viana, A., et al., 2009. Solid pure component property effects on modeling upper crossover pressure for supercritical fluid process synthesis: A case study for the separation of Annatto pigments using SC-CO2. The Journal of Supercritical Fluids. 49, 1–8. https://doi.org/10.1016/j.supflu.2008.12.006.

Del Valle, J.M., Aguilera, J.M., 1988. An improved equation for predicting the solubility of vegetable oils in supercritical carbon dioxide. Industrial & Engineering Chemistry Research. 27, 1551–1553. https://doi.org/10.1021/ie00080a036.

Demirtas, C., Dilek, C., 2019. Enhanced solubility of siloxy-modified polyhedral oligomeric silsesquioxanes in supercritical carbon dioxide. The Journal of Supercritical Fluids. 143, 358–364. https://doi.org/10.1016/j.supflu.2018.09.015.

Duarte, R.C.F., Moreira, P.S.S., Ferreira, C.N., et al., 2020. Atrial Fibrillation and use of rivaroxaban: performance of the prothrombin time/INR as a function of time after blood collection. International Journal of Cardiovascular Sciences. 34, 116–121. https://doi.org/10.36660/ijcs.20190141.

Duereh, A., Smith Jr, R.L., 2018. Strategies for using hydrogen-bond donor/acceptor solvent pairs in developing green chemical processes with supercritical fluids. The Journal of Supercritical Fluids. 141, 182–197. https://doi.org/10.1016/j.supflu.2017.11.004.

Esfandiari, N., 2015. Production of micro and nano particles of pharmaceutical by supercritical carbon dioxide. The Journal of Supercritical Fluids. 100, 129–141. https://doi.org/10.1016/j.supflu.2014.12.028.

Esfandiari, N., Ali Sajadian, S., 2022. Solubility of Lacosamide in supercritical carbon Dioxide: An experimental analysis and thermodynamic modeling. Journal of Molecular Liquids. 360, 119467. https://doi.org/10.1016/j.molliq.2022.119467.

Esfandiari, N., Ghoreishi, S.M., 2013. Synthesis of 5-fluorouracil nanoparticles via supercritical gas antisolvent process. The Journal of Supercritical Fluids. 84, 205–210. https://doi.org/10.1016/j.supflu.2013.10.008.

Esfandiari, N., Ghoreishi, S.M., 2014. Kinetic Modeling of the Gas Antisolvent Process for Synthesis of 5-Fluorouracil Nanoparticles. Chemical Engineering & Technology. 37, 73–80. https://doi.org/10.1002/ceat.201300431.

Esfandiari, N., Ghoreishi, S.M., 2015a. Ampicillin nanoparticles production via supercritical CO2 gas antisolvent process. Aaps Pharmscitech. 16, 1263–1269. https://doi.org/10.1208/s12249-014-0264-y.

Esfandiari, N., Ghoreishi, S.M., 2015b. Optimal thermodynamic conditions for ternary system (CO2, DMSO, ampicillin) in supercritical CO2 antisolvent process. Journal of the Taiwan Institute of Chemical Engineers. 50, 31–36. https://doi.org/10.1016/j.jtice.2014.12.015.

Esfandiari, N., Sajadian, S.A., 2022a. CO2 Utilization as Gas Antisolvent for the Pharmaceutical Micro and Nanoparticle Production: A Review. Arabian Journal of Chemistry. 104164 https://doi.org/10.1016/j.arabjc.2022.104164.

Esfandiari, N., Saadati Ardestani, N., Alwi, R.S., et al., 2023. Solubility measurement of verapamil for the preparation of developed nanomedicines using supercritical fluid. Scientific Reports. 13, 17089. https://doi.org/10.1038/s41598-023-44280-7.

Esfandiari, N., Sajadian, S.A., 2022b. Experimental and modeling investigation of Glibenclamide solubility in supercritical carbon dioxide. Fluid Phase Equilibria. 556, 113408. https://doi.org/10.1016/j.fluid.2022.113408.

Evans, A., Davies, M., Osborne, V., et al., 2020. Evaluation of the incidence of bleeding in patients prescribed rivaroxaban for the treatment and prevention of deep vein thrombosis and pulmonary embolism in UK secondary care: an observational cohort study. BMJ Open. 10, e038102.

Fernandez, S., Lenoir, C., Samer, C.F., et al., 2021. Drug-Drug Interactions Leading to Adverse Drug Reactions with Rivaroxaban: A Systematic Review of the Literature and Analysis of VigiBase. Journal of Personalized Medicine. 11, 250. https://doi.org/10.3390/jpm11040250.

Galiuto, L., Patrono, C., 2021. Rivaroxaban, a novel option for patients with atrial fibrillation and a bioprosthetic mitral valve. European Heart Journal. https://doi.org/10.1093/eurheartj/ehaa1075.

Garlapati, C. and G. Madras, 2010. New empirical expressions to correlate solubilities of solids in supercritical carbon dioxide. Thermochimica Acta. 500, 123-127. ttps://doi.org/10.1016/j.tca.2009.12.004.

González, J.C., Vieytes, M.R., Botana, A.M., et al., 2001. Modified mass action law-based model to correlate the solubility of solids and liquids in entrained supercritical carbon dioxide. Journal of Chromatography a. 910, 119–125. https://doi.org/10.1016/s0021-9673(00)01120-1.

Gordillo, M., Blanco, M., Molero, A., et al., 1999. Solubility of the antibiotic Penicillin G in supercritical carbon dioxide. The Journal of Supercritical Fluids. 15, 183–190. https://doi.org/10.1016/s0896-8446(99)00008-x.

Gross, J., 2005. An equation-of-state contribution for polar components: Quadrupolar molecules. AIChE Journal. 51, 2556–2568. https://doi.org/10.1002/aic.10502.

Gross, J., Sadowski, G., 2001. Perturbed-chain SAFT: An equation of state based on a perturbation theory for chain molecules. Industrial & Engineering Chemistry Research. 40, 1244–1260. https://doi.org/10.1021/ie0003887.

Güçlü-Üstündağ, Ö., Temelli, F., 2005. Solubility behavior of ternary systems of lipids, cosolvents and supercritical carbon dioxide and processing aspects. The Journal of Supercritical Fluids. 36, 1–15. https://doi.org/10.1016/j.supflu.2005.03.002.

Han, S., Wang, W., Jiao, Z., et al., 2017. Solubility of vitamin E acetate in supercritical carbon dioxide: measurement and correlation. Journal of Chemical & Engineering Data. 62, 3854–3860. https://doi.org/10.1021/acs.jced.7b00550.

Hani, U., Alosaimi, H.E., Huwaimel, B., et al., 2023. Study of hyoscine solubility in scCO2: Experimental measurement and thermodynamic modeling. Journal of Molecular Liquids. 381, 121821. https://doi.org/10.1016/j.molliq.2023.121821.

Hazaveie, S.M., Sodeifian, G., Sajadian, S.A., 2020. Measurement and thermodynamic modeling of solubility of Tamsulosin drug (anti cancer and anti-prostatic tumor

activity) in supercritical carbon dioxide. The Journal of Supercritical Fluids. 163, 104875. https://doi.org/10.1016/j.supflu.2020.104875.
Hojjati, M., Yamini, Y., Khajeh, M., et al., 2007. Solubility of some statin drugs in supercritical carbon dioxide and representing the solute solubility data with several density-based correlations. The Journal of Supercritical Fluids. 41, 187–194. https://doi.org/10.1016/j.supflu.2006.10.006.
Honarvar, B., Sajadian, S.A., Rojas, A., et al., 2023. Solubility and thermodynamic modeling of sildenafil citrate in supercritical carbon dioxide. Fluid Phase Equilibria. 566, 113677. https://doi.org/10.1016/j.fluid.2022.113677.
Hosseini, S.Z., Bozorgmehr, M.R., Masrurnia, M., et al., 2018. Study of the effects of methanol, ethanol and propanol alcohols as co-solvents on the interaction of methimazole, propranolol and phenazopyridine with carbon dioxide in supercritical conditions by molecular dynamics. The Journal of Supercritical Fluids. 140, 91–100. https://doi.org/10.1016/j.supflu.2018.06.005.
Jash, A., Hatami, T., Rizvi, S.S., 2020. Phosphatidylcholine solubility in supercritical carbon dioxide: Experimental data, thermodynamic modeling, and application in bioactive-encapsulated liposome synthesis. The Journal of Supercritical Fluids. 158, 104720. https://doi.org/10.1016/j.supflu.2019.104720.
Jeffrey, G.A., Jeffrey, G.A., 1997. An introduction to hydrogen bonding. Oxford University Press, New York.
Jouyban, A., Chan, H.-K., Foster, N.R., 2002a. Mathematical representation of solute solubility in supercritical carbon dioxide using empirical expressions. The Journal of Supercritical Fluids. 24, 19–35. https://doi.org/10.1016/s0896-8446(02)00015-3.
Jouyban, A., Rehman, M., Shekunov, B.Y., et al., 2002b. Solubility prediction in supercritical CO2 using minimum number of experiments. Journal of Pharmaceutical Sciences. 91, 1287–1295. https://doi.org/10.1002/jps.10127.
Kalikin, N., Kurskaya, M., Ivlev, D., et al., 2020. Carbamazepine solubility in supercritical CO2: A comprehensive study. Journal of Molecular Liquids. 311, 113104. https://doi.org/10.1016/j.molliq.2020.113104.
Kalikin, N., Oparin, R., Kolesnikov, A., et al., 2021. A crossover of the solid substances solubility in supercritical fluids: What is it in fact? Journal of Molecular Liquids. 334, 115997. https://doi.org/10.1016/j.molliq.2021.115997.
Keshmiri, K., Vatanara, A., Yamini, Y., 2014. Development and evaluation of a new semi-empirical model for correlation of drug solubility in supercritical CO2. Fluid Phase Equilibria. 363, 18–26. https://doi.org/10.1016/j.fluid.2013.11.013.
Khansary, M.A., Amiri, F., Hosseini, A., et al., 2015. Representing solute solubility in supercritical carbon dioxide: A novel empirical model. Chemical Engineering Research and Design. 93, 355–365. https://doi.org/10.1016/j.cherd.2014.05.004.
Khudaida, S.H., Chen, Y.-M., Zheng, Y.-F., et al., 2023a. Solid solubility measurement of haloperidol in supercritical carbon dioxide and nanonization using the rapid expansion of supercritical solutions process. The Journal of Supercritical Fluids. 192, 105785. https://doi.org/10.1016/j.supflu.2022.105785.
Khudaida, S.H., Hsieh, W.-Y., Huang, Y.-Z., et al., 2023b. Solubility of probenecid in supercritical carbon dioxide and composite particles prepared using supercritical antisolvent process. The Journal of Supercritical Fluids. 194, 105851. https://doi.org/10.1016/j.supflu.2023.105851.
Knez, Z., e., D. Cör and M. a. Knez Hrnčič, 2017. Solubility of solids in sub-and supercritical fluids: a review 2010–2017. Journal of Chemical & Engineering Data. 63, 860–884. https://doi.org/10.1021/acs.jced.7b00778.
Kostrzewa, D., Dobrzyńska-Inger, A., Turczyn, A., 2019. Experimental data and modelling of the solubility of high-carotenoid paprika extract in supercritical carbon dioxide. Molecules. 24, 4174. https://doi.org/10.3390/molecules24224174.
Kubitza, D., Becka, M., Mueck, W., et al., 2010. Effects of renal impairment on the pharmacokinetics, pharmacodynamics and safety of rivaroxaban, an oral, direct Factor Xa inhibitor. British Journal of Clinical Pharmacology. 70, 703–712. https://doi.org/10.1111/j.1365-2125.2010.03753.x.
Kumar, S.K., Johnston, K.P., 1988. Modelling the solubility of solids in supercritical fluids with density as the independent variable. The Journal of Supercritical Fluids. 1, 15–22. https://doi.org/10.1016/0896-8446(88)90005-8.
Kushwah, V., Arora, S., Tamás Katona, M., et al., 2021. On Absorption Modeling and Food Effect Prediction of Rivaroxaban, a BCS II Drug Orally Administered as an Immediate-Release Tablet. Pharmaceutics. 13, 283. https://doi.org/10.3390/pharmaceutics13020283.
Li, B., Guo, W., Ramsey, E.D., 2017. Determining the solubility of nifedipine and quinine in supercritical fluid carbon dioxide using continuously stirred static solubility apparatus interfaced with online supercritical fluid chromatography. Journal of Chemical & Engineering Data. 62, 1530–1537. https://doi.org/10.1021/acs.jced.7b00012.
Li, Q., Zhang, Z., Zhong, C., et al., 2003. Solubility of solid solutes in supercritical carbon dioxide with and without cosolvents. Fluid Phase Equilibria. 207, 183–192. https://doi.org/10.1016/s0378-3812(03)00022-0.
Li, G., Zhou, D., Xu, Q.-Q., et al., 2018. Solubility of ionic liquid [Bmim] Ac in supercritical CO2 containing different cosolvents. Journal of Chemical & Engineering Data. 63, 1596–1602. https://doi.org/10.1021/acs.jced.7b01108.
MacEachern, L., Kermanshahi-pour, A., Mirmehrabi, M., 2020. Supercritical carbon dioxide for pharmaceutical co-crystal production. Crystal Growth & Design. 20, 6226–6244. https://doi.org/10.1021/acs.cgd.0c00571.
Mahesh, G., Garlapati, C., 2022. Modelling of Solubility of Some Parabens in Supercritical Carbon Dioxide and New Correlations. Arabian Journal for Science and Engineering. 47, 5533–5545. https://doi.org/10.1007/s13369-021-05500-2.
Majrashi, M., Salah Al-Shati, A., Grishina, M., et al., 2023. Experimental measurement and thermodynamic modeling of Chlorothiazide solubility in supercritical carbon dioxide. Case Studies in Thermal Engineering. 41, 102621. https://doi.org/10.1016/j.csite.2022.102621.
Manna, L., Banchero, M., 2018. Solubility of tolbutamide and chlorpropamide in supercritical carbon dioxide. Journal of Chemical & Engineering Data. 63, 1745–1751. https://doi.org/10.1021/acs.jced.8b00050.
Maqbool, W., Hobson, P., Dunn, K., et al., 2017. Supercritical carbon dioxide separation of carboxylic acids and phenolics from bio-oil of lignocellulosic origin: understanding bio-oil compositions, compound solubilities, and their fractionation. Industrial & Engineering Chemistry Research. 56, 3129–3144. https://doi.org/10.1021/acs.iecr.6b04111.
Matin, M.M., Uzzaman, M., Chowdhury, S.A., et al., 2022. In vitro antimicrobial, physicochemical, pharmacokinetics and molecular docking studies of benzoyl uridine esters against SARS-CoV-2 main protease. Journal of Biomolecular Structure and Dynamics. 40, 3668–3680. https://doi.org/10.1080/07391102.2020.1850358.
Méndez-Santiago, J., Teja, A.S., 1999. The solubility of solids in supercritical fluids. Fluid Phase Equilibria. 158, 501–510. https://doi.org/10.1016/S0378-3812(99)00154-5.
Mueck, W., Stampfuss, J., Kubitza, D., et al., 2014. Clinical pharmacokinetic and pharmacodynamic profile of rivaroxaban. Clinical Pharmacokinetics. 53, 1–16. https://doi.org/10.1007/s40262-013-0100-7.
Naikoo, G.A., Saeedi Zadegan, M., Zamani Pedram, M., et al., 2021. Solubility of vitamin A in supercritical CO2: experimental study and thermodynamic modeling. Scientific Reports. 11, 1–13. https://doi.org/10.1038/s41598-021-92374-x.
Najafi, M., Esfandiari, N., Honarvar, B., et al., 2021. Production of Rosuvastatin Calcium Nanoparticles Using Gas Antisolvent Technique: Experimental and Optimization. Periodica Polytechnica. Chemical Engineering. 65, 442–453. https://doi.org/10.3311/ppch.16629.
Nateghi, H., Sodeifian, G., Razmimanesh, F., et al., 2023. A machine learning approach for thermodynamic modeling of the statically measured solubility of nilotinib hydrochloride monohydrate (anti-cancer drug) in supercritical CO2. Scientific Reports. 13, 12906. https://doi.org/10.1038/s41598-023-40231-4.
Notej, B., Bagheri, H., Alsaikhan, F., et al., 2023. Increasing solubility of phenytoin and raloxifene drugs: Application of supercritical CO2 technology. Journal of Molecular Liquids. 373, 121246. https://doi.org/10.1016/j.molliq.2023.121246.
Ongkasin, K., Sauceau, M., Masmoudi, Y., et al., 2019. Solubility of cefuroxime axetil in supercritical CO2: Measurement and modeling. The Journal of Supercritical Fluids. 152, 104498. https://doi.org/10.1016/j.supflu.2019.03.010.
Padrela, L., Rodrigues, M.A., Duarte, A., et al., 2018. Supercritical carbon dioxide-based technologies for the production of drug nanoparticles/nanocrystals–a comprehensive review. Advanced Drug Delivery Reviews. 131, 22–78. https://doi.org/10.1016/j.addr.2018.07.010.
Patel, M.R., Mahaffey, K.W., Garg, J., et al., 2011. Rivaroxaban versus warfarin in nonvalvular atrial fibrillation. New England Journal of Medicine. 365, 883–891. https://doi.org/10.1056/nejmoa1009638.
Peng, D.-Y., Robinson, D.B., 1976. A new two-constant equation of state. Industrial & Engineering Chemistry Fundamentals. 15, 59–64. https://doi.org/10.1021/i160057a011.
Peyrovedin, H., Shariati, A., 2020. Polar Hard-Core Exponential-6 Intermolecular Potential Function for Determining the Thermodynamic Properties of Polar Gases. Industrial & Engineering Chemistry Research. 59, 14106–14114. https://doi.org/10.1021/acs.iecr.0c01465.
Pishnamazi, M., Zabihi, S., Jamshidian, S., et al., 2020a. Thermodynamic modelling and experimental validation of pharmaceutical solubility in supercritical solvent. Journal of Molecular Liquids. 319, 114120. https://doi.org/10.1016/j.molliq.2020.114120.
Pishnamazi, M., Zabihi, S., Jamshidian, S., et al., 2020b. Measuring solubility of a chemotherapy-anti cancer drug (busulfan) in supercritical carbon dioxide. Journal of Molecular Liquids. 317, 113954. https://doi.org/10.1016/j.molliq.2020.113954.
Pishnamazi, M., Zabihi, S., Sarafzadeh, P., et al., 2020c. Using static method to measure tolmetin solubility at different pressures and temperatures in supercritical carbon dioxide. Scientific Reports. 10, 1–7. https://doi.org/10.1038/s41598-020-76330-9.
Pishnamazi, M., Hosseini, S., Zabihi, S., et al., 2021a. Chloroquine (antimalaria medication with anti SARS-CoV activity) solubility in supercritical carbon dioxide. Journal of Molecular Liquids. 322, 114539. https://doi.org/10.1016/j.molliq.2020.114539.
Pishnamazi, M., Zabihi, S., Jamshidian, S., et al., 2021b. Experimental and thermodynamic modeling decitabine anti cancer drug solubility in supercritical carbon dioxide. Scientific Reports. 11, 1–8. https://doi.org/10.1038/s41598-020-80399-7.
Pitchaiah, K., Rao, C.B., Sivaraman, N., et al., 2017. Solubility of dialkylalkyl phosphonates in supercritical carbon dioxide: Experimental and modeling approach. Fluid Phase Equilibria. 435, 88–97. https://doi.org/10.1016/j.fluid.2016.12.011.
Pitchaiah, K., Lamba, N., Sivaraman, N., et al., 2018. Solubility of trioctylmethylammonium chloride in supercritical carbon dioxide and the influence of co-solvents on the solubility behavior. The Journal of Supercritical Fluids. 138, 102–114. https://doi.org/10.1016/j.supflu.2018.04.002.
Prausnitz, J., Lichtenthaler, R., Azevedo, E., 1999. Molecular Thermodynamics of Fluid Phase Equilibria, 3rd edn. Prentice Hall PTR, Englewood Cliffs.
Reddy, S.N., Madras, G., 2011. A new semi-empirical model for correlating the solubilities of solids in supercritical carbon dioxide with cosolvents. Fluid Phase Equilibria. 310, 207–212. https://doi.org/10.1016/j.fluid.2011.08.021.
Rojas, A., Sajadian, S.A., López-de-Dicastillo, C., et al., 2023. Improving and measuring the solubility of favipiravir and montelukast in SC-CO 2 with ethanol projecting their nanonization. RSC Advances. 13, 34210–34223. https://doi.org/10.1039/d3ra05484e.
Saadati Ardestani, N., Amani, M., Moharrery, L., 2020. Determination of Anthraquinone Violet 3RN solubility in supercritical carbon dioxide with/without co-solvent: Experimental data and modeling (empirical and thermodynamic models). Chemical Engineering Research and Design. 159, 529–542. https://doi.org/10.1016/j.cherd.2020.04.026.

Saadati Ardestani, N., Sajadian, S.A., Rojas, A., et al., 2023. Solubility of famotidine in supercritical carbon dioxide: Experimental measurement and thermodynamic modeling. The Journal of Supercritical Fluids. 201, 106031. https://doi.org/10.1016/j.supflu.2023.106031.

Sajadian, S.A., Amani, M., Saadati Ardestani, N., et al., 2022a. Experimental analysis and thermodynamic modelling of lenalidomide solubility in supercritical carbon dioxide. Arabian Journal of Chemistry. 15, 103821. https://doi.org/10.1016/j.arabjc.2022.103821.

Sajadian, S.A., Ardestani, N.S., Esfandiari, N., et al., 2022b. Solubility of favipiravir (as an anti-COVID-19) in supercritical carbon dioxide: An experimental analysis and thermodynamic modeling. The Journal of Supercritical Fluids. 183, 105539. https://doi.org/10.1016/j.supflu.2022.105539.

Sajadian, S.A., Ardestani, N.S., Jouyban, A., 2022c. Solubility of montelukast (as a potential treatment of COVID -19) in supercritical carbon dioxide: Experimental data and modelling. Journal of Molecular Liquids. 349, 118219. https://doi.org/10.1016/j.molliq.2021.118219.

Sajadian, S.A., Peyrovedin, H., Zomorodian, K., et al., 2023. Using the supercritical carbon dioxide as the solvent of Nystatin: Studying the effect of co-solvent, experimental and correlating. The Journal of Supercritical Fluids. 194, 105858. https://doi.org/10.1016/j.supflu.2023.105858.

Samama, M.M., Contant, G., Spiro, T.E., et al., 2013. Laboratory assessment of rivaroxaban: a review. Thrombosis Journal. 11, 1–7. https://doi.org/10.1186/1477-9560-11-11.

Sauceau, M., Letourneau, J.-J., Richon, D., et al., 2003. Enhanced density-based models for solid compound solubilities in supercritical carbon dioxide with cosolvents. Fluid Phase Equilibria. 208, 99–113. https://doi.org/10.1016/s0378-3812(03)00005-0.

Seshamamba, B., Sekaran, C., 2017. Spectrophotometric quantification of direct factor xa inhibitor, rivaroxaban, in raw and tablet dosage form. Glob Drugs and Therap. 2, 1–8. https://doi.org/10.15761/gdt.1000122.

Shi, K., Feng, L., He, L., et al., 2017. Solubility determination and correlation of gatifloxacin, enrofloxacin, and ciprofloxacin in supercritical CO2. Journal of Chemical & Engineering Data. 62, 4235–4243. https://doi.org/10.1021/acs.jced.7b00601.

Soave, G., 1972. Equilibrium constants from a modified Redlich-Kwong equation of state. Chemical Engineering Science. 27, 1197–1203. https://doi.org/10.1016/0009-2509(72)80096-4.

Sodeifian, G., Razmimanesh, F., Sajadian, S.A., 2019e. Solubility measurement of a chemotherapeutic agent (Imatinib mesylate) in supercritical carbon dioxide: Assessment of new empirical model. The Journal of Supercritical Fluids. 146, 89–99. https://doi.org/10.1016/j.supflu.2019.01.006.

Sodeifian, G., Saadati Ardestani, N., Sajadian, S.A., 2019f. Solubility measurement of a pigment (Phthalocyanine green) in supercritical carbon dioxide: Experimental correlations and thermodynamic modeling. Fluid Phase Equilibria. 494, 61–73. https://doi.org/10.1016/j.fluid.2019.04.024.

Sodeifian, G., Garlapati, C., Hazaveie, S.M., et al., 2020a. Solubility of 2, 4, 7-Triamino-6-phenylpteridine (Triamterene, Diuretic Drug) in supercritical carbon dioxide: experimental data and modeling. Journal of Chemical & Engineering Data. 65, 4406–4416. https://doi.org/10.1021/acs.jced.0c00268.

Sodeifian, G., Razmimanesh, F., Ardestani, N.S., et al., 2020b. Experimental data and thermodynamic modeling of solubility of Azathioprine, as an immunosuppressive and anti-cancer drug, in supercritical carbon dioxide. Journal of Molecular Liquids. 299, 112179. https://doi.org/10.1016/j.molliq.2019.112179.

Sodeifian, G., Razmimanesh, F., Sajadian, S.A., 2020c. Prediction of solubility of sunitinib malate (an anti-cancer drug) in supercritical carbon dioxide (SC–CO2): experimental correlations and thermodynamic modeling. Journal of Molecular Liquids. 297, 111740. https://doi.org/10.1016/j.molliq.2019.111740.

Sodeifian, G., Razmimanesh, F., Sajadian, S.A., et al., 2020d. Experimental data and thermodynamic modeling of solubility of Sorafenib tosylate, as an anti-cancer drug, in supercritical carbon dioxide: Evaluation of Wong-Sandler mixing rule. The Journal of Chemical Thermodynamics. 142, 105998. https://doi.org/10.1016/j.jct.2019.105998.

Sodeifian, G., Saadati Ardestani, N., Razmimanesh, F., et al., 2020e. Experimental and thermodynamic analyses of supercritical CO2-Solubility of minoxidil as an antihypertensive drug. Fluid Phase Equilibria. 522, 112745. https://doi.org/10.1016/j.fluid.2020.112745.

Sodeifian, G., Sajadian, S.A., 2018. Solubility measurement and preparation of nanoparticles of an anticancer drug (Letrozole) using rapid expansion of supercritical solutions with solid cosolvent (RESS-SC). The Journal of Supercritical Fluids. 133, 239–252. https://doi.org/10.1016/j.supflu.2017.10.015.

Sodeifian, G., Sajadian, S.A., Ardestani, N.S., 2017a. Determination of solubility of Aprepitant (an antiemetic drug for chemotherapy) in supercritical carbon dioxide: empirical and thermodynamic models. The Journal of Supercritical Fluids. 128, 102–111. https://doi.org/10.1016/j.supflu.2017.05.019.

Sodeifian, G., Sajadian, S.A., Razmimanesh, F., 2017b. Solubility of an antiarrhythmic drug (amiodarone hydrochloride) in supercritical carbon dioxide: experimental and modeling. Fluid Phase Equilibria. 450, 149–159. https://doi.org/10.1016/j.fluid.2017.07.015.

Sodeifian, G., Ardestani, N.S., Sajadian, S.A., et al., 2018a. Measurement, correlation and thermodynamic modeling of the solubility of Ketotifen fumarate (KTF) in supercritical carbon dioxide: evaluation of PCP-SAFT equation of state. Fluid Phase Equilibria. 458, 102–114. https://doi.org/10.1016/j.fluid.2017.11.016.

Sodeifian, G., Razmimanesh, F., Sajadian, S.A., et al., 2018b. Solubility measurement of an antihistamine drug (Loratadine) in supercritical carbon dioxide: Assessment of qCPA and PCP-SAFT equations of state. Fluid Phase Equilibria. 472, 147–159. https://doi.org/10.1016/j.fluid.2018.05.018.

Sodeifian, G., Ardestani, N.S., Sajadian, S.A., et al., 2019a. Experimental measurements and thermodynamic modeling of Coumarin-7 solid solubility in supercritical carbon dioxide: Production of nanoparticles via RESS method. Fluid Phase Equilibria. 483, 122–143. https://doi.org/10.1016/j.fluid.2018.11.006.

Sodeifian, G., Detakhsheshpour, R., Sajadian, S.A., 2019b. Experimental study and thermodynamic modeling of Esomeprazole (proton-pump inhibitor drug for stomach acid reduction) solubility in supercritical carbon dioxide. The Journal of Supercritical Fluids. 154, 104606. https://doi.org/10.1016/j.supflu.2019.104606.

Sodeifian, G., Hazaveie, S.M., Sajadian, S.A., et al., 2019c. Experimental investigation and modeling of the solubility of oxcarbazepine (an anticonvulsant agent) in supercritical carbon dioxide. Fluid Phase Equilibria. 493, 160–173. https://doi.org/10.1016/j.fluid.2019.04.013.

Sodeifian, G., Hazaveie, S.M., Sajadian, S.A., et al., 2019d. Determination of the solubility of the repaglinide drug in supercritical carbon dioxide: Experimental data and thermodynamic modeling. Journal of Chemical & Engineering Data. 64, 5338–5348. https://doi.org/10.1021/acs.jced.9b00550.

Sodeifian, G., Saadati Ardestani, N., Sajadian, S.A., et al., 2020f. Prediction of solubility of sodium valproate in supercritical carbon dioxide: experimental study and thermodynamic modeling. Journal of Chemical & Engineering Data. 65, 1747–1760. https://doi.org/10.1021/acs.jced.9b01069.

Sodeifian, G., Sajadian, S.A., Derakhsheshpour, R., 2020g. Experimental measurement and thermodynamic modeling of Lansoprazole solubility in supercritical carbon dioxide: Application of SAFT-VR EoS. Fluid Phase Equilibria. 507, 112422. https://doi.org/10.1016/j.fluid.2019.112422.

Sodeifian, G., Alwi, R.S., Razmimanesh, F., et al., 2021a. Solubility of Quetiapine hemifumarate (antipsychotic drug) in supercritical carbon dioxide: Experimental, modeling and Hansen solubility parameter application. Fluid Phase Equilibria. 537, 113003. https://doi.org/10.1016/j.fluid.2021.113003.

Sodeifian, G., Garlapati, C., Razmimanesh, F., et al., 2021b. Measurement and modeling of clemastine fumarate (antihistamine drug) solubility in supercritical carbon dioxide. Scientific Reports. 11, 24344. https://doi.org/10.1038/s41598-021-03596-y.

Sodeifian, G., Garlapati, C., Razmimanesh, F., et al., 2021c. Solubility of amlodipine besylate (calcium channel blocker drug) in supercritical carbon dioxide: Measurement and correlations. Journal of Chemical & Engineering Data. 66, 1119–1131. https://doi.org/10.1021/acs.jced.0c00913.

Sodeifian, G., Garlapati, C., Razmimanesh, F., et al., 2021d. The solubility of Sulfabenzamide (an antibacterial drug) in supercritical carbon dioxide: Evaluation of a new thermodynamic model. Journal of Molecular Liquids. 335, 116446. https://doi.org/10.1016/j.molliq.2021.116446.

Sodeifian, G., Hazaveie, S.M., Sodeifian, F., 2021e. Determination of Galantamine solubility (an anti-alzheimer drug) in supercritical carbon dioxide (CO2): Experimental correlation and thermodynamic modeling. Journal of Molecular Liquids. 330, 115695. https://doi.org/10.1016/j.molliq.2021.115695.

Sodeifian, G., Nasri, L., Razmimanesh, F., et al., 2021f. Measuring and modeling the solubility of an antihypertensive drug (losartan potassium, Cozaar) in supercritical carbon dioxide. Journal of Molecular Liquids. 331, 115745. https://doi.org/10.1016/j.molliq.2021.115745.

Sodeifian, G., Sajadian, S.A., Razmimanesh, F., et al., 2021g. Solubility of Ketoconazole (antifungal drug) in SC-CO2 for binary and ternary systems: Measurements and empirical correlations. Scientific Reports. 11, 1–13. https://doi.org/10.1038/s41598-021-87243-6.

Sodeifian, G., Alwi, R.S., Razmimanesh, F., 2022a. Solubility of Pholcodine (antitussive drug) in supercritical carbon dioxide: Experimental data and thermodynamic modeling. Fluid Phase Equilibria. 556, 113396. https://doi.org/10.1016/j.fluid.2022.113396.

Sodeifian, G., Alwi, R.S., Razmimanesh, F., et al., 2022b. Solubility of pazopanib hydrochloride (PZH, anticancer drug) in supercritical CO2: Experimental and thermodynamic modeling. The Journal of Supercritical Fluids. 190, 105759. https://doi.org/10.1016/j.supflu.2022.105759.

Sodeifian, G., Garlapati, C., Razmimanesh, F., et al., 2022c. Experimental solubility and thermodynamic modeling of empagliflozin in supercritical carbon dioxide. Scientific Reports. 12, 9008. https://doi.org/10.1038/s41598-022-12769-2.

Sodeifian, G., Garlapati, C., Razmimanesh, F., et al., 2022d. Solubility measurement and thermodynamic modeling of pantoprazole sodium sesquihydrate in supercritical carbon dioxide. Scientific Reports. 12, 7758. https://doi.org/10.1038/s41598-022-11887-1.

Sodeifian, G., Garlapati, C., Roshanghias, A., 2022e. Experimental solubility and modeling of Crizotinib (anti-cancer medication) in supercritical carbon dioxide. Scientific Reports. 12, 1–16. https://doi.org/10.1038/s41598-022-22366-y.

Sodeifian, G., Hsieh, C.-M., Derakhsheshpour, R., et al., 2022f. Measurement and modeling of metoclopramide hydrochloride (anti-emetic drug) solubility in supercritical carbon dioxide. Arabian Journal of Chemistry. 103876 https://doi.org/10.1016/j.arabjc.2022.103876.

Sodeifian, G., Nasri, L., Razmimanesh, F., et al., 2022g. CO2 utilization for determining solubility of teriflunomide (immunomodulatory agent) in supercritical carbon dioxide: Experimental investigation and thermodynamic modeling. Journal of CO2 Utilization. 58, 101931. https://doi.org/10.1016/j.jcou.2022.101931.

Sodeifian, G., Surya Alwi, R., Razmimanesh, F., et al., 2022h. Solubility of Dasatinib monohydrate (anticancer drug) in supercritical CO2: Experimental and thermodynamic modeling. Journal of Molecular Liquids. 346, 117899. https://doi.org/10.1016/j.molliq.2021.117899.

Sodeifian, G., Surya Alwi, R., Razmimanesh, F., et al., 2022i. Solubility of prazosin hydrochloride (alpha blocker antihypertensive drug) in supercritical CO2: Experimental and thermodynamic modelling. Journal of Molecular Liquids. 362, 119689. https://doi.org/10.1016/j.molliq.2022.119689.

Sodeifian, G., Arbab Nooshabadi, M., Razmimanesh, F., et al., 2023a. Solubility of buprenorphine hydrochloride in supercritical carbon dioxide: Study on experimental measuring and thermodynamic modeling. Arabian Journal of Chemistry. 16, 105196. https://doi.org/10.1016/j.arabjc.2023.105196.

Sodeifian, G., Garlapati, C., Arbab Nooshabadi, M., et al., 2023b. Solubility measurement and modeling of hydroxychloroquine sulfate (antimalarial medication) in supercritical carbon dioxide. Scientific Reports. 13, 8112. https://doi.org/10.1038/s41598-023-34900-7.

Sodeifian, G., Hsieh, C.-M., Tabibzadeh, A., et al., 2023c. Solubility of palbociclib in supercritical carbon dioxide from experimental measurement and Peng-Robinson equation of state. Scientific Reports. 13, 2172. https://doi.org/10.1038/s41598-023-29228-1.

Sodeifian, G., Nasri, L., Razmimanesh, F., et al., 2023d. Solubility of ibrutinib in supercritical carbon dioxide (Sc-CO2): Data correlation and thermodynamic analysis. The Journal of Chemical Thermodynamics. 182, 107050. https://doi.org/10.1016/j.jct.2023.107050.

Sodeifian, G., Usefi, M.M.B., Razmimanesh, F., et al., 2023e. Determination of the solubility of rivaroxaban (anticoagulant drug, for the treatment and prevention of blood clotting) in supercritical carbon dioxide: Experimental data and correlations. Arabian Journal of Chemistry. 16, 104421. https://doi.org/10.1016/j.arabjc.2022.104421.

Soltani, S., Mazloumi, S.H., 2017. A new empirical model to correlate solute solubility in supercritical carbon dioxide in presence of co-solvent. Chemical Engineering Research and Design. 125, 79–87. https://doi.org/10.1016/j.cherd.2017.07.006.

Span, R., Wagner, W., 1996. A new equation of state for carbon dioxide covering the fluid region from the triple-point temperature to 1100 K at pressures up to 800 MPa. Journal of Physical and Chemical Reference Data. 25, 1509–1596. https://doi.org/10.1063/1.555991.

Sparks, D.L., Hernandez, R., Estévez, L.A., 2008. Evaluation of density-based models for the solubility of solids in supercritical carbon dioxide and formulation of a new model. Chemical Engineering Science. 63, 4292–4301. https://doi.org/10.1016/j.ces.2008.05.031.

Sridar, R., Bhowal, A., Garlapati, C., 2013. A new model for the solubility of dye compounds in supercritical carbon dioxide. Thermochimica Acta. 561, 91–97. https://doi.org/10.1016/j.tca.2013.03.029.

Sung, H.-D., Shim, J.-J., 1999. Solubility of CI disperse red 60 and CI disperse blue 60 in supercritical carbon dioxide. Journal of Chemical & Engineering Data. 44, 985–989. https://doi.org/10.1021/je990018t.

Tabernero, A., del Valle, E.M.M., Galán, M.Á., 2010. A comparison between semiempirical equations to predict the solubility of pharmaceutical compounds in supercritical carbon dioxide. The Journal of Supercritical Fluids. 52, 161–174. https://doi.org/10.1016/j.supflu.2010.01.009.

Tamura, K., Alwi, R.S., Tanaka, T., et al., 2017. Solubility of 1-aminoanthraquinone and 1-nitroanthraquinone in supercritical carbon dioxide. The Journal of Chemical Thermodynamics. 104, 162–168. https://doi.org/10.1016/j.jct.2016.09.032.

Thomas, T.F., Ganetsky, V., Spinler, S.A., 2013. Rivaroxaban: an oral factor Xa inhibitor. Clinical Therapeutics. 35, 4–27. https://doi.org/10.1016/j.clinthera.2012.12.005.

Tsai, C.-C., Lin, H.-M., Lee, M.-J., 2017. Phase equilibrium and micronization for flufenamic acid with supercritical carbon dioxide. Journal of the Taiwan Institute of Chemical Engineers. 72, 19–28. https://doi.org/10.1016/j.jtice.2017.01.011.

Venkatesan, K., Alshahrani, S.M., Alsubaiyel, A.M., et al., 2022. Experimental-Theoretical approach for determination of Metformin solubility in supercritical carbon dioxide: Thermodynamic modeling. Case Studies in Thermal Engineering. 102649 https://doi.org/10.1016/j.csite.2022.102649.

Wang, S.-W., Chang, S.-Y., Hsieh, C.-M., 2021. Measurement and modeling of solubility of gliclazide (hypoglycemic drug) and captopril (antihypertension drug) in supercritical carbon dioxide. The Journal of Supercritical Fluids. 174, 105244. https://doi.org/10.1016/j.supflu.2021.105244.

Wang, B.-C., Su, C.-S., 2020. Solid solubility measurement of ipriflavone in supercritical carbon dioxide and microparticle production through the rapid expansion of supercritical solutions process. Journal of CO2 Utilization. 37, 285–294. https://doi.org/10.1016/j.jcou.2019.12.012.

Xiang, S.-T., Chen, B.-Q., Kankala, R.K., et al., 2019. Solubility measurement and RESOLV-assisted nanonization of gambogic acid in supercritical carbon dioxide for cancer therapy. The Journal of Supercritical Fluids. 150, 147–155. https://doi.org/10.1016/j.supflu.2019.04.008.

Yan, J., Du, S., Du, H., et al., 2022. Comparison of Four Density-Based Semi-Empirical Models for the Solubility of Azo Disperse Dyes in Supercritical Carbon Dioxide. Processes. 10, 1960. https://doi.org/10.3390/pr10101960.

Yeoh, H.S., Chong, G.H., Azahan, N.M., et al., 2013. Solubility measurement method and mathematical modeling in supercritical fluids. Engineering Journal. 17, 67–78. https://doi.org/10.4186/ej.2013.17.3.67.

Yu, Z.-R., Singh, B., Rizvi, S.S., et al., 1994. Solubilities of fatty acids, fatty acid esters, triglycerides, and fats and oils in supercritical carbon dioxide. The Journal of Supercritical Fluids. 7, 51–59. https://doi.org/10.1016/0896-8446(94)90006-x.

Zabihi, S., Esmaeili-Faraj, S.H., Borousan, F., et al., 2020a. Loxoprofen solubility in supercritical carbon dioxide: experimental and modeling approaches. Journal of Chemical & Engineering Data. 65, 4613–4620. https://doi.org/10.1021/acs.jced.0c00470.

Zabihi, S., Rahnama, Y., Sharafi, A., et al., 2020b. Experimental solubility measurements of fenoprofen in supercritical carbon dioxide. Journal of Chemical & Engineering Data. 65, 1425–1434. https://doi.org/10.1021/acs.jced.9b00861.

Zabihi, S., Jamshidian, S., Borousan, F., et al., 2021a. Measuring salsalate solubility in supercritical carbon dioxide: experimental and thermodynamic modelling. The Journal of Chemical Thermodynamics. 152, 106271. https://doi.org/10.1016/j.jct.2020.106271.

Zabihi, S., Khoshmaram, A., Pishnamazi, M., et al., 2021b. Thermodynamic study on solubility of brain tumor drug in supercritical solvent: Temozolomide case study. Journal of Molecular Liquids. 321, 114926. https://doi.org/10.1016/j.molliq.2020.114926.

Zha, X., Han, S., Wang, W., et al., 2019. Experimental measurement and correlation of solubility of ethosuximide in supercritical carbon dioxide. The Journal of Chemical Thermodynamics. 131, 104–110. https://doi.org/10.1016/j.jct.2018.10.032.

Zhan, S., Li, S., Zhao, Q., et al., 2017. Measurement and correlation of curcumin solubility in supercritical carbon dioxide. Journal of Chemical & Engineering Data. 62, 1257–1263. https://doi.org/10.1021/acs.jced.6b00798.

Zhan, S., Miao, H., Zhao, Y., et al., 2020. Experimental Determination and Association Model for the Solubility of Laminarin in Supercritical Carbon Dioxide. Journal of Chemical & Engineering Data. 65, 1814–1823. https://doi.org/10.1021/acs.jced.9b01084.